

AD-A243 950



✓  
2

PL-TR-91-2239

CALCULATION AND MODELING OF THE ATTITUDE FOR THE  
COMBINED RELEASE AND RADIATION EFFECTS SATELLITE

W. J. McNeil

Radex, Inc.  
Three Preston Court  
Bedford, MA 01730



September 26, 1991

Scientific Report No. 8

Approved for public release; distribution unlimited



PHILLIPS LABORATORY  
AIR FORCE SYSTEMS COMMAND  
HANSCOM AIR FORCE BASE, MASSACHUSETTS 01731-5000

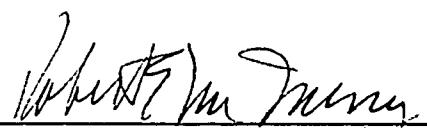
91-19181



91 1227 053

"This technical report has been reviewed and is approved for publication"

  
EDWARD C. ROBINSON  
Contract Manager  
Data Analysis Division

  
ROBERT E. MCINERNEY, Director  
Data Analysis Division

This report has been reviewed by the ESD Public Affairs Office (PA) and is releasable to the National Technical Information Service (NTIS).

Qualified requestors may obtain additional copies from the Defense Technical Information Center. All others should apply to the National Technical Information Service.

If your address has changed, or if you wish to be removed from the mailing list, or if the addressee is no longer employed by your organization, please notify GL/IMA, Hanscom AFB, MA 01731. This will assist us in maintaining a current mailing list.

Do not return copies of this report unless contractual obligations or notices on a specific document requires that it be returned.

REPORT DOCUMENTATION PAGE

1a. REPORT SECURITY CLASSIFICATION <b>Unclassified</b>		1b. RESTRICTIVE MARKINGS	
2a. SECURITY CLASSIFICATION AUTHORITY		3. DISTRIBUTION / AVAILABILITY OF REPORT Approved for Public Release Distribution Unlimited	
2b. DECLASSIFICATION / DOWNGRADING SCHEDULE			
4. PERFORMING ORGANIZATION REPORT NUMBER(S) <b>RX-R-91092</b>		5. MONITORING ORGANIZATION REPORT NUMBER(S) <b>PL-TR-91-2239</b>	
6a. NAME OF PERFORMING ORGANIZATION <b>RADEX, Inc.</b>	6b. OFFICE SYMBOL (if applicable)	7a. NAME OF MONITORING ORGANIZATION <b>Phillips Laboratory</b>	
6c. ADDRESS (City, State, and ZIP Code) <b>Three Preston Court Bedford, MA 01730</b>		7b. ADDRESS (City, State, and ZIP Code) <b>Hanscom AFB Massachusetts 01731-5000</b>	
8a. NAME OF FUNDING / SPONSORING ORGANIZATION	8b. OFFICE SYMBOL (if applicable)	9. PROCUREMENT INSTRUMENT IDENTIFICATION NUMBER <b>Contract F19628-89-C-0068</b>	
8c. ADDRESS (City, State, and ZIP Code)		10. SOURCE OF FUNDING NUMBERS	
		PROGRAM ELEMENT NO. <b>62101F</b>	PROJECT NO. <b>7659</b>
		TASK NO. <b>05</b>	WORK UNIT ACCESSION NO. <b>AB</b>
11. TITLE (Include Security Classification) <b>Calculation and Modeling of the Attitude for the Combined Release and Radiation Effects Satellite</b>			
12. PERSONAL AUTHOR(S) <b>W. J. McNeil</b>			
13a. TYPE OF REPORT <b>Scientific Report #8</b>	13b. TIME COVERED FROM <b>6/89</b> TO <b>9/91</b>	14. DATE OF REPORT (Year, Month, Day) <b>1991, September 26</b>	15. PAGE COUNT <b>54</b>
16. SUPPLEMENTARY NOTATION			
17. COSATI CODES		18. SUBJECT TERMS (Continue on reverse if necessary and identify by block number)	
FIELD	GROUP	SUB-GROUP	
		<b>Attitude determination, Attitude modeling, CRRES attitude</b>	
19. ABSTRACT (Continue on reverse if necessary and identify by block number) Algorithms are presented for the calculation and modeling of the attitude for the Combined Release and Radiation Effects Satellite. Examples of typical attitude behavior are given and comparisons with fluxgate magnetometer data are used to estimate error in the attitude model under various conditions. It is found that for the vast majority of orbits, error levels are below 2°. Immediately after attitude adjustments, errors may reach 10° and the orbit following an adjust may have errors of up to 5° in the very small segments. During these periods, the error level in the model is of about the same magnitude as the deviation of the attitude from pure rotation. A description of the dynamical response of the satellite to various mission events is also included as well as a list of mission events through Orbit 800.			
20. DISTRIBUTION / AVAILABILITY OF ABSTRACT <input checked="" type="checkbox"/> UNCLASSIFIED/UNLIMITED <input type="checkbox"/> SAME AS RPT. <input type="checkbox"/> DTIC USERS		21. ABSTRACT SECURITY CLASSIFICATION <b>Unclassified</b>	
22a. NAME OF RESPONSIBLE INDIVIDUAL <b>E. C. Robinson</b>		22b. TELEPHONE (Include Area Code) <b>(617)377-3840</b>	22c. OFFICE SYMBOL <b>PL/GPD</b>

## ACKNOWLEDGMENTS

The CRRES Attitude Determination Program was written by Rick Porter, Rich Harada and Rich Schuster of Space Applications Corp., Sunnyvale, Calif. Techniques for refitting the results of this program and interactive modeling of the attitude are described in the present document. These needs arose as the result of work to analyze the CRRES fluxgate magnetometer data, in support of Howard Singer of PHG, whom we also thank for access to the magnetometer data used here for error estimates. We wish as well to acknowledge Robert McNerney and Al Griffin of GPD, who guided the development and testing of both the original attitude system and the fitting software. The subroutines SYMBOL and NUMBER used in some of the graphics displays are products of Tektronix, Inc. The subroutines APCH and APFS used in attitude modeling are products of IMSL, Inc. All are used with permission.

Accession For	
NTIS CRA&I	<input checked="" type="checkbox"/>
DTIC TAB	<input type="checkbox"/>
Unannounced	<input type="checkbox"/>
Justification .....	
By .....	
Distribution /	
Availability Codes	
Dist	Availability / or Special
A-1	



## TABLE OF CONTENTS

1. Introduction .....	1
2. Attitude Determination .....	2
2.1 Instrumentation .....	2
2.2 Telemetry Processing .....	4
2.3 Observation Sets .....	5
2.4 Spin Rate .....	6
2.5 First Guess Attitude .....	7
2.6 Attitude State Vectors .....	10
2.7 CADP Segmentation and Fitting .....	14
3. CRRES Attitude Characteristics .....	15
3.1 A Typical Orbit .....	15
3.2 CADP Fit Results .....	17
3.3 Constraints .....	19
4. Attitude Modeling .....	22
4.1 Spin Axis Vector .....	22
4.2 Spin Rate .....	23
4.3 Eclipse Model .....	25
4.4 Segmentation .....	26
4.5 Results .....	27
5. Error Estimates .....	31
5.1 Nominal Orbits .....	31
5.2 Attitude Adjust Orbits .....	31
5.3 Other Anomalies .....	37
5.4 Summary .....	38
6. Anomalies .....	40
6.1 Clock Jumps .....	40
6.2 Attitude Adjustments .....	41
6.3 Spin Rate Changes .....	41
6.4 Canister Releases .....	41
6.5 Orbit Adjusts .....	42
References .....	43
Appendix. History of Mission Events .....	A-1

## LIST OF FIGURES

1. The CRRES Attitude Instruments .....	3
2. Determination of the Attitude Vector .....	8
3. Original CADP First Guess .....	11
4. First Guess as Presently Calculated .....	12
5. Attitude Characteristics .....	16
6. Original CADP Attitude Model for Orbit 313 .....	18
7. Original Model compared to IGRF for Orbit 313 .....	20
8. Present Attitude Model for Orbit 313 .....	28
9. Present Model compared to IGRF for Orbit 313 .....	29
10. Model for Orbit 795 compared to IGRF .....	30
11. Sun Declination Measurements after an Attitude Adjust .....	33
12. Model for Orbit 820 compared to IGRF .....	34
13. Model for Orbit 821 compared to IGRF .....	35
14. Model for Orbit 822 compared to IGRF .....	36
15. Survey of Accuracy for Orbits 600-700 .....	39

## LIST OF TABLES

1. Possible CRRES Observation Sets .....	5
2. Mission Event Codes .....	42

## 1. INTRODUCTION

The Combined Release and Radiation Effects Satellite (CRRES) is a spin stabilized spacecraft in a near equatorial eccentric orbit, with perigee around 350 kilometers and apogee near 33,500 kilometers. The CRRES attitude is essential for conversion of magnetometer data to geophysical coordinates and for the interpretation of solar panel, photometer and other experiments on board. The satellite is equipped with a sun sensor, a horizon sensor and a low resolution magnetometer for use in attitude determination. With proper treatment, these instruments are capable at present of resolving the attitude of the spacecraft to better than  $2^\circ$ .

The CRRES Attitude Determination Program (CADP) was developed by Space Applications Corporation [1989] and delivered in July 1989, almost a year before launch of the satellite. The attitude determination and modeling routines were designed for nominal operations of the spacecraft. Although the actual definition of 'nominal operations' has, to our knowledge, never been clearly set down, one can infer the requirements from the design specifications of the original CADP. These limitations include (a) pure rotation around the spacecraft z-axis, (b) adequacy of the averaged spin rate calculated from sun sensor data for *linear* representation of the phase during each period or *segment* delineated for modeling attitude, and (c) high accuracy in the engineering magnetometer.

Upon delivery, Radex undertook the responsibility for integration of the system into the overall Orbital Data Processing (ODP) program and for monitoring the performance. Before launch, it became apparent from simulated data that the linear model of the phase would be severely limiting for some applications. Even with a constant spin rate, propagation of errors in spin axis position and natural motion of the sun in the defining coordinate system gave rise to a drift in the calculated spin rate and required two-hour segmentation with approximately one-half degree discontinuities at segment boundaries. To remove this limitation, an attitude refitting program was developed [McNeil, 1990] to use the calculated phase to find a spin rate correction term. Originally, this was intended to be used only to reprocess the attitude for use in magnetic field despinning. However, shortly after launch, it became apparent that specifying a constant spin rate even under normal operation would lead to unacceptable errors. It was also clear that the calculation of attitude from magnetometer data was inadequate except for short periods around perigee.

In response to these problems, the attitude refitting system was enhanced to include a linear and eventually a quadratic spin rate during sunlit periods and a quadratic spin rate during eclipse. Also, a global spin axis pointing direction was determined using sun and horizon sensor data alone. This software has been used exclusively in the generation of the CRRES attitude model. The modeling is done interactively from intermediate results of the original CADP, and the model coefficients generated by the CADP are discarded. Integration of the revised model into the batch processing of attitude has never been attempted for a variety of reasons. First, times for attitude adjustments, spin rate changes and other anomalies are not generally available at run time and determination of these events is quite easily accomplished from inspection of the intermediate attitude data. Also, telemetry anomalies and missing data can be more easily dealt with by interactive segmentation. Finally, the interactive fitting requires little extra time for all but the most difficult orbits, and the system's presentation graphics provides a high degree of quality control.

This document is meant to serve several purposes. At present, the only formal documentation of the attitude determination algorithms is a design specification written in Program Design Language (commonly called PDL). In this form, it is extremely difficult to follow the calculations from beginning to end. Thus it seems valuable for future reference to describe the calculations in more concise mathematical terms, albeit that most are relatively standard. Second, there is a need to document the changes made to the system since delivery and especially the attitude modeling software. Third, it seems valuable to present some firm accuracy estimates for the attitude. Finally, this seems a good medium for the presentation of some of the idiosyncracies of the CRRES attitude behavior to serve as a guide in thinking about attitude software development for similar missions.

In Section 2, the attitude instrumentation for CRRES is briefly described and the algorithms for calculation of spacecraft spin axis pointing direction and spin phase from simultaneous observations are presented. Next, we discuss the specific problems encountered in the generation of the attitude model and the solutions presently in place. Finally, we describe the anomalies one might encounter in the use of the CRRES attitude model and discuss the magnitude of uncertainty to be expected.

## 2. ATTITUDE DETERMINATION

This section describes the instruments and algorithms used to determine an 'instantaneous' attitude point for the satellite. The CRRES attitude is defined in Earth Centered Inertial (ECI) coordinates. In ECI, the z-axis is collinear with the Earth's rotation axis and the x-axis points toward the vernal equinox in the ecliptic plane. The attitude is defined by the right ascension and declination of the spin axis (the CRRES z-axis) and by a phase which is measured in the spacecraft spin plane relative to passage of the spacecraft x-axis through the ECI xy-plane traveling northward. The attitude 'point' is comprised of the right ascension  $\alpha$  and declination  $\delta$  of the spin axis, an instantaneous spin rate  $\omega$ , and a time  $t_n$  at which the spin phase was zero.

### 2.1 INSTRUMENTATION

In this discussion, the attitude instrumentation aboard the satellite will be described only to the extent needed to understand the data obtained from them. Details of the instruments themselves have been given elsewhere [Ball, 1986a,b,c]. The CRRES attitude instruments are shown schematically in Figure 1. The sun sensor consists of a fan located parallel to the spin axis on the negative x side of the spacecraft. Each time the sun passes through the fan, the angle between the spin axis and the sun is determined to an accuracy of  $\pm 0.5^\circ$ . Also, the time of the crossing of the sun through the spacecraft xy-plane,  $t_{ss}$ , is determined. This time is inserted into telemetry in a rather complex way, as are the other event times discussed below. The details of this, which will be avoided here, are available in Ball Aerospace documentation [1985].

The attitude magnetometer, referred to as the engineering magnetometer in what follows to differentiate it from the science magnetometer, is tri-axial and aligned with the spacecraft axes to better than  $0.2^\circ$ . It samples the field approximately once per second in two gain states, one with resolution of

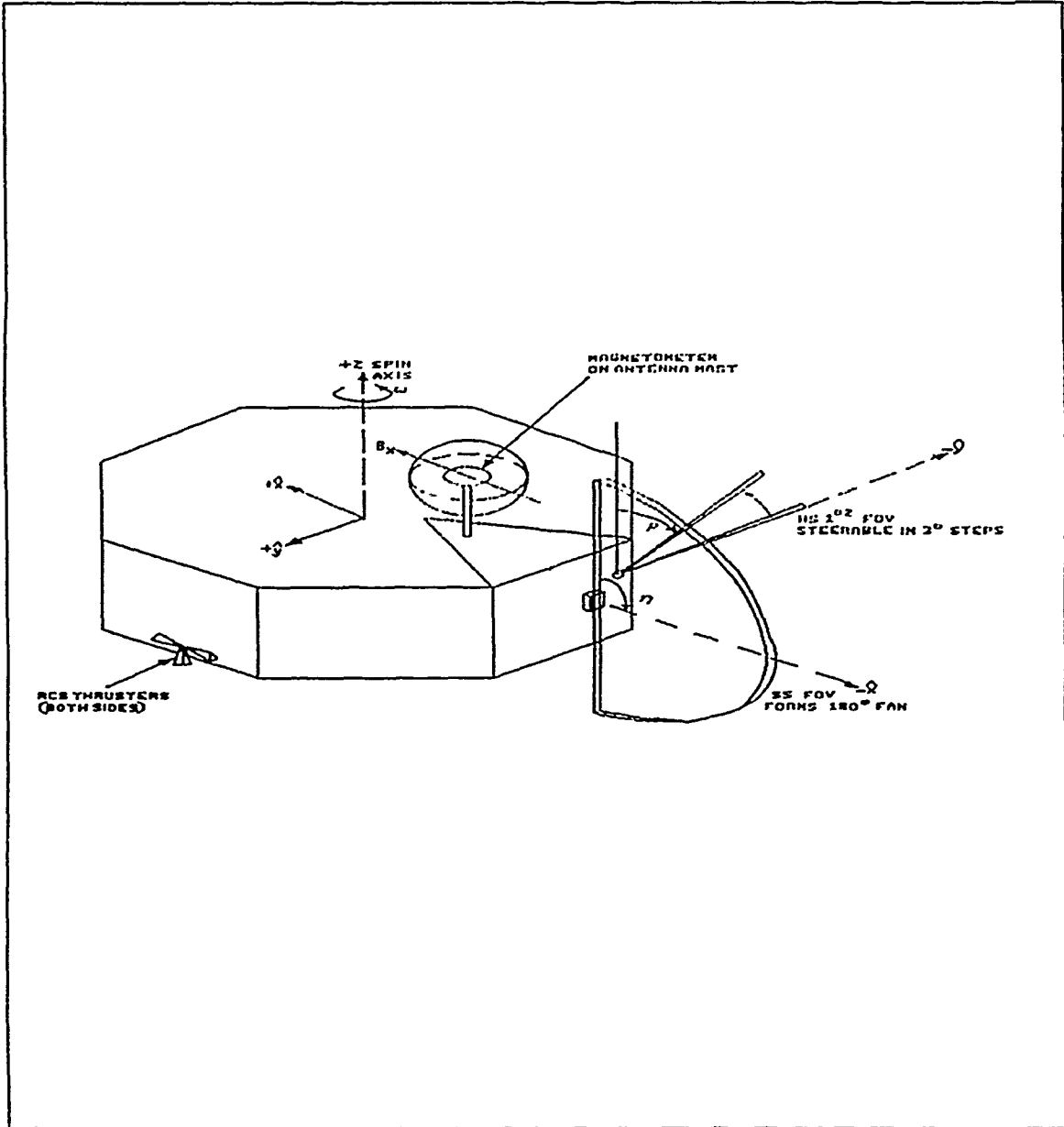


Figure 1. The CRRES Attitude Determination Instruments.

approximately 480 nT and another with approximately 74 nT resolution. Also, the time  $t_{\text{mag}}$  at which the field along the magnetometer x-axis is zero is determined and inserted into telemetry.

The Earth horizon sensor provides the times that the 50% radiance point of the Earth's IR horizon crosses the sensor's field of view. These are separated into leading edge,  $t_{\text{HSLE}}$ , and trailing edge,  $t_{\text{HSTE}}$ . Contrary to the depiction in Figure 1, the horizon sensor is now permanently fixed in the spacecraft spin plane and is not steerable.

## 2.2 TELEMETRY PROCESSING

The first step in attitude determination for CRRES is the unpacking, time-tagging and conversion to physical units of the raw attitude telemetry values. The data file used is a reduced version of the total telemetry containing data from the three attitude instruments only. Each Master Frame (MF) in this file has been time tagged with the Universal Time (UT) at the start of the master frame by the Master Frame Formatting (MFF) program. The processing of the sun sensor data requires the conversion of the measured sun declination angle from its 'grey scale' code to degrees [McNeil and McInerney, 1988] and the calculation of the 'absolute' UT of the sun hit.

Time tagging of the sun pulse is identical to that of the horizon sensor and magnetometer zero crossing data. These are derived from a local time counter with a resolution of 64 kHz. The local clock is reset to zero at the master frame sync pulse. The pulse occurs 1.5 ms *before* the start of each master frame. When a sensor event occurs, the value of the local clock is latched by the appropriate holding register. This value remains constant in the register until the next such event occurs and is dumped twice per major frame. In order to determine the actual time of a sensor event, one first examines the values of successive data to see when a change in the value has taken place. One must next determine if the local clock time refers to the present or the previous master frame. For example, the first of the two sun pulses is read out in word 62 of subframe 1. There are 32 subframes per master frame (numbered 0 through 31) and 256 words per subframe (numbered 0 through 255). The readout time of the first sun pulse, relative to the MF time, is

$$t_r = 0.128 (1 + 62/256) \text{ sec.}$$

at the nominal rate of 4.096 seconds/MF. The value of the local time clock is found from

$$t_c = .0000625N - .0015 \text{ sec.}$$

where N is the clock count, and the difference between MF sync pulse and the actual start of the MF has been subtracted to make  $t_c$  relative to the start of the MF. If  $t_c$  is *less* than  $t_r$  then the readout must have pertained to the current master frame, and the time of the crossing is given by

$$t_{\text{SS}} = t_{\text{MF}} + t_c$$

where  $t_{\text{SS}}$  is the assigned time of the current master frame. Otherwise, the time is given by

$$t_{\text{SS}} = t_{\text{MF}} + t_c - 4.096 \text{ sec.}$$

Additionally, the horizon sensor has an additional built-in delay time  $t_d$  which must be added to the time as calculated above. This time is taken to be 645.55 ms for 2 rpm mode and 51.54 ms for 10 rpm mode.

Finally, the analog readings of the engineering magnetometer are converted to the magnetic field values along the three spacecraft principal axes.

### 2.3 OBSERVATION SETS

From the calibrated telemetry data, a series of observation sets is next formed. Each of these constitute data taken during one spin period. Some of these sets contain pairs of observations from which the attitude can be calculated in several different ways. Others contain insufficient data to calculate it even once. Observation sets are defined from one sun hit to the next or, in eclipse, from one crossing of the magnetic field zero to another. For the CRRES instruments, the possible combination of measurements is given in Table 1.

Table 1. Possible CRRES Observation Sets

#	Sensors	When Applicable
1	SS Alone	Never (0%)
2	HS Alone	Never (0%)
3	SS,HS	Never (0%)
4	Mag Alone	Typical Eclipse (8%)
5	SS, Mag	Full Sun, Earth not in HS FOV (75%)
6	HS, Mag	Occasionally during Eclipse (2%)
7	SS, HS, Mag	Full Sun, Earth in HS FOV (15%)

The first four of these events are, as indicated, not applicable to the way in which the CRRES data is currently processed. Had the use of the magnetic field been optionally limited to the regions very close to the earth, the majority of the data would have been of type 1. For reasons treated in more detail later, we have chosen not to limit the use of the magnetometer at this level. The percentages given above apply roughly to typical orbits during the first six months or so of the mission. As can be seen, only a relatively small portion of the data contains earth sightings.

## 2.4 SPIN RATE

From comparing the time of each observation set with that of the next, assuming both are defined by a sun or magnetometer zero cross pair, the instantaneous spin rate is determined. The calculation for sun crossing pairs is straightforward. That for magnetometer zero cross pairs is equally so except for a correction term added later that deserves mention. The correction can be carried out only when an estimate is available for the spin axis pointing direction,  $z_{\text{est}}$ . In the CRRES package, the estimate used is that of the first guess attitude, the calculation of which is explained below. The correction goes as follows. The ECI unit vectors of the model field at the first zero cross,  $b_1$  and the second zero cross,  $b_2$  are found. Taking the cross product of each with the spin axis gives two vectors,  $c_1$  and  $c_2$  which are equivalent in phase to the projection of the magnetic field into the spin plane at the times of the zero crossings. Taking the phase angle between  $c_1$  and  $c_2$  gives a correction term for the spin rate deduced from the two, representing the motion of the background field between the two zero crossings. Specifically, if  $\omega_{\text{mag}}$  is the spin rate found from subtracting times for two successive zero crossings, then the corrected spin rate

$$\omega_{\text{mag}}' = \omega_{\text{mag}} / (1 - \theta/2\pi)$$

where  $\theta$  is the rotation angle from  $c_1$  to  $c_2$ . This rotation angle is calculated from the law of cosines. Since this particular transformation will come up again in what follows, we define the rotation angle about the vector  $a$  from the projection of vector  $b$  into the plane perpendicular to  $a$  to the projection of the vector  $c$  into the same plane,  $\Lambda(a,b,c)$ , on the interval  $[0,2\pi]$  as follows.

$$\cos\psi = \frac{b \cdot c - (a \cdot c)(b \cdot a)}{[1 - (a \cdot b)^2]^{1/2} [1 - (a \cdot c)^2]^{1/2}} \quad (1)$$

$$\begin{aligned} \Lambda(a,b,c) &= \cos^{-1}(\cos\psi) & c \cdot (a \times b) &> 0 \\ \Lambda(a,b,c) &= 2\pi - \cos^{-1}(\cos\psi) & c \cdot (a \times b) &< 0 \end{aligned}$$

The complement operation above simply puts the angle in the proper quadrant. In the calculation above,  $\theta = \Lambda(z_{\text{est}}, c_1, c_2)$ . Whenever a proper spin rate cannot be calculated for an observation set, the so called telemetered spin rate is substituted. The telemetered spin rate is calculated on board from an average of the last sixty sun hits.

## 2.5 FIRST GUESS ATTITUDE

For each pair of observations in each set, two distinct spin axis pointing directions can be calculated. In order to determine which one is correct, one must do some sort of survey of a large number of points taken from different positions in an orbit or from different sensors. The false solution will drift as the objects sensed change orientation in the spacecraft frame while the true solution will remain relatively constant. For CRRES, this is done by calculating the spin axis pointing direction  $z$  from the first one-hundred observations using the sun sensor data plus  $t_{HSLE}$ ,  $t_{HSTE}$  and  $t_{mag}$ . These are calculated as follows.

*Sun Sensor/Magnetometer Attitude.* Using the times of sun hit and magnetic field zero cross, we find the rotation angle between the sun and the spacecraft x-axis at the time of the zero cross

$$\Phi = 2\pi\omega(t_{mag} - t_{SS})$$

The angular separation between the x-axis and the sun at the zero cross is given by the law of cosines, which reduces here to

$$\cos\eta = \sin\beta\cos\Phi$$

where  $\beta$  is the sun aspect angle. We find two possible ECI pointing directions for the spacecraft x-axis using the ECI model reference vectors for the sun  $s$  and magnetic field  $b$  by taking the interception of two cones around  $s$  and  $b$  with half-vertex angles  $\eta$  and  $\pi/2$  respectively.

A general method [Wertz, 1986] is as follows. Suppose the vectors  $e$  and  $s$  have aspect angles  $\eta$  and  $\beta$  respectively. This is shown schematically in Figure 2. We take

$$\begin{aligned} x &= \frac{\cos\beta - e \cdot s \cos\eta}{1 - (e \cdot s)^2} \\ y &= \frac{\cos\eta - e \cdot s \cos\beta}{1 - (e \cdot s)^2} \end{aligned} \quad (2)$$

$$z = \pm \sqrt{\frac{1 - x \cos\beta - y \cos\eta}{1 - (e \cdot s)^2}}$$

Then, forming

$$c = s \times e$$

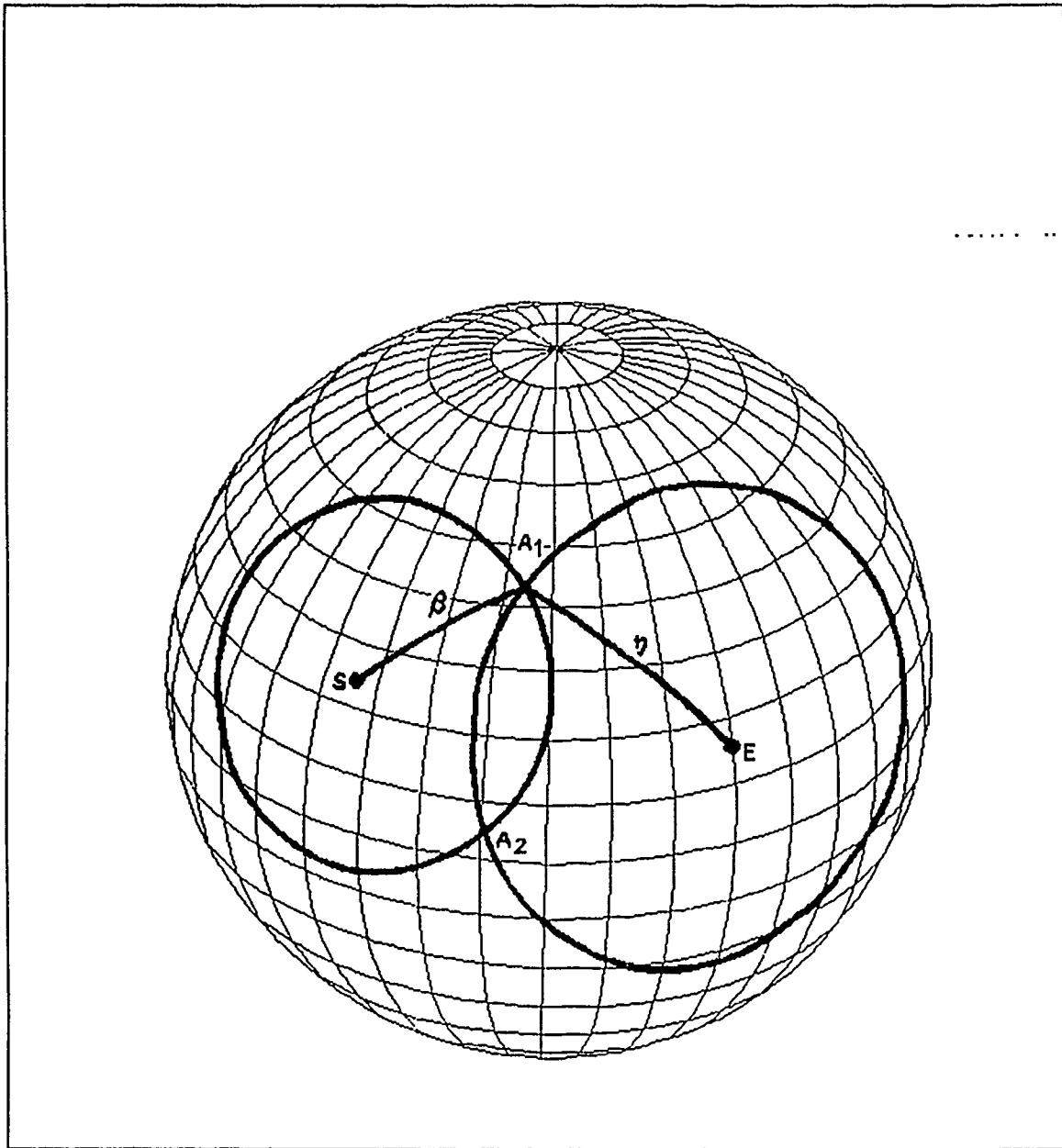


**Figure 2.** Determination of degenerate attitude vector using two known vectors and two arc length measurements. From *Wertz* [1986].

we find the interception vectors from

$$a = xs + ye + zc$$

We refer to this calculation in what follows as the function  $\Xi(e, \eta, s, \beta)$ . In the calculation of the auxiliary reference vectors above, we have

$$h_{1,2} = \Xi(s, \eta, b, \pi/2)$$

From here, two possible spin axis pointing directions are calculated by finding the interception of the sun vector  $s$  with half-vertex angle  $\beta$  and the vectors  $h_{1,2}$  again with vertex angle  $\pi/2$ . This gives a total of four calculated spin axis pointing directions in all.

$$\begin{aligned} z_{1a,b} &= \Xi(h_1, \pi/2, s, \beta) \\ z_{2a,b} &= \Xi(h_2, \pi/2, s, \beta) \end{aligned}$$

From each pair, say  $z_{1a,b}$ , there will be one that does not reproduce the measured rotation angle. By examining the rotation angle

$$\alpha = \Lambda(z_{1a}, s, h_1)$$

in comparison to the measured angle  $\Phi$ , we can tell which one to accept, thus reducing the total number of solutions to two.

*Sun Sensor/Horizon Sensor Attitude.* For sun with earth leading or trailing edge calculations, a spherical earth is assumed for first guess attitude. The apparent radius of the earth's CO<sub>2</sub> horizon is calculated from

$$\rho = \sin^{-1}[(r_e + r_{CO_2})/r_{sat}]$$

where  $r_e$  is the mean radius of the earth,  $r_{CO_2}$  is the altitude of the CO<sub>2</sub> horizon, taken as 40 km, and  $r_{sat}$  is the length of the satellite to earth vector. The angular separation between the reference vector (horizon sensor) and the sun is again found from the law of cosines,

$$\cos \eta = \cos \beta \cos \gamma + \sin \beta \sin \gamma \cos \Phi$$

where  $\beta$  is the sun aspect angle,  $\gamma$  is the horizon sensor cant angle (which is  $\pi/2$  in practice but variable in the code) and  $\Phi$  is the rotation angle between sun and earth hits. We find two possible horizon sensor vectors from the ECI sun vector  $s$  and the satellite-to-earth vector  $e$  by intersecting the cones  $\eta$  away from  $s$  and  $\rho$  away from  $e$ .

$$h_{1,2} = \Xi(s, \eta, e, \rho)$$

Then, the four possible spin axis positions are found from

$$\begin{aligned} z_{1a,b} &= \Xi(s, \beta, h_1, \gamma) \\ z_{2a,b} &= \Xi(s, \beta, h_2, \gamma) \end{aligned}$$

and, as before, one of each pair is eliminated by examination of the rotation angle.

*First Guess Histogram.* From the first 100 attitude points calculated, a histogram is constructed to determine the first guess attitude. Originally, more than one first guess interval was possible during a single orbit. Additional first guess intervals were added at times of attitude adjusts. However, lack of knowledge of mission events prior to execution of the attitude calculation forced this approach to be abandoned. This could have been a serious problem except for the fact that the pre-adjust and post-adjust attitudes are close enough so that the same first guess works equally well for both. This is a result of the CRRES attitude itself. Since the spin axis points nearly at the sun and since the sun drifts counterclockwise looking down the ECI z-axis, the spacecraft spin axis will 'trail' the sun. The sun drifts away from the spin axis to the maximum allowed angle of around  $15^\circ$ . Then a series of precession maneuvers are performed to push the spin axis back to about  $5^\circ$ . Since the two possible solutions using sun data are on opposite sides of the sun and since the post-adjust spin axis attitude is on the same side as the pre-adjust attitude, the post-adjust true solution is closer to the first guess for the pre-adjust attitude than is the false solution. It is therefore selected using the pre-adjust first guess.

The solutions are binned by an angle defined by the rotation angle between the attitude solution  $z$  around the mean sun vector for the orbit  $s$  from a vector close to the ECI  $z$ -axis. Because the CRRES spin axis points nearly toward the sun, this scheme works nicely for attitude points determined from horizon sensor data. However, because the magnetic field is nearly perpendicular to the satellite-to-sun vector, true and false solutions derived from magnetic field zero crossings alone tend to form equal histograms on both sides of the sun. Originally, the program took the first 100 points only, not generally including horizon sensor data. Because of this, ambiguous histograms and incorrect first guesses often resulted. This situation is quite serious since it could result in incorrect choice of the spin axis pointing direction throughout the orbit. We found a solution by restricting the first guess histogram calculation to observation sets containing earth limb data. A comparison of histograms with and without this restriction is given in Figure 3 and Figure 4.

First guess determination using magnetic field data alone is not able to reliably differentiate between the true and false solutions. In this case, the most populated bin would indeed have been the correct one, but in other cases this is not true. Even this case is rather too close for comfort with the most populous bin only about 20% more frequent than one far from the actual solution. These histogram plots are produced from the attitude modeling and quality control program developed by Radex, Inc. Plots like this are viewed for each orbit processed in order to assure an adequate first guess.

## 2.6 ATTITUDE STATE VECTORS

Once the first guess for the spin axis pointing direction has been determined, each pair of useful observations in each of the observation sets is used to calculate a two-fold degenerate 'instantaneous' spin axis pointing vector at the time of the observation set. The first guess is used to choose the correct attitude from this set and the attitude state vector for the observation set is calculated from a weighted average of all calculations made within that set. The weighting factors are three in number and are defined in the CADP input. There is one for the sun sensor, one for the magnetometer and a third for the horizon sensor. The average state vector is calculated as follows.

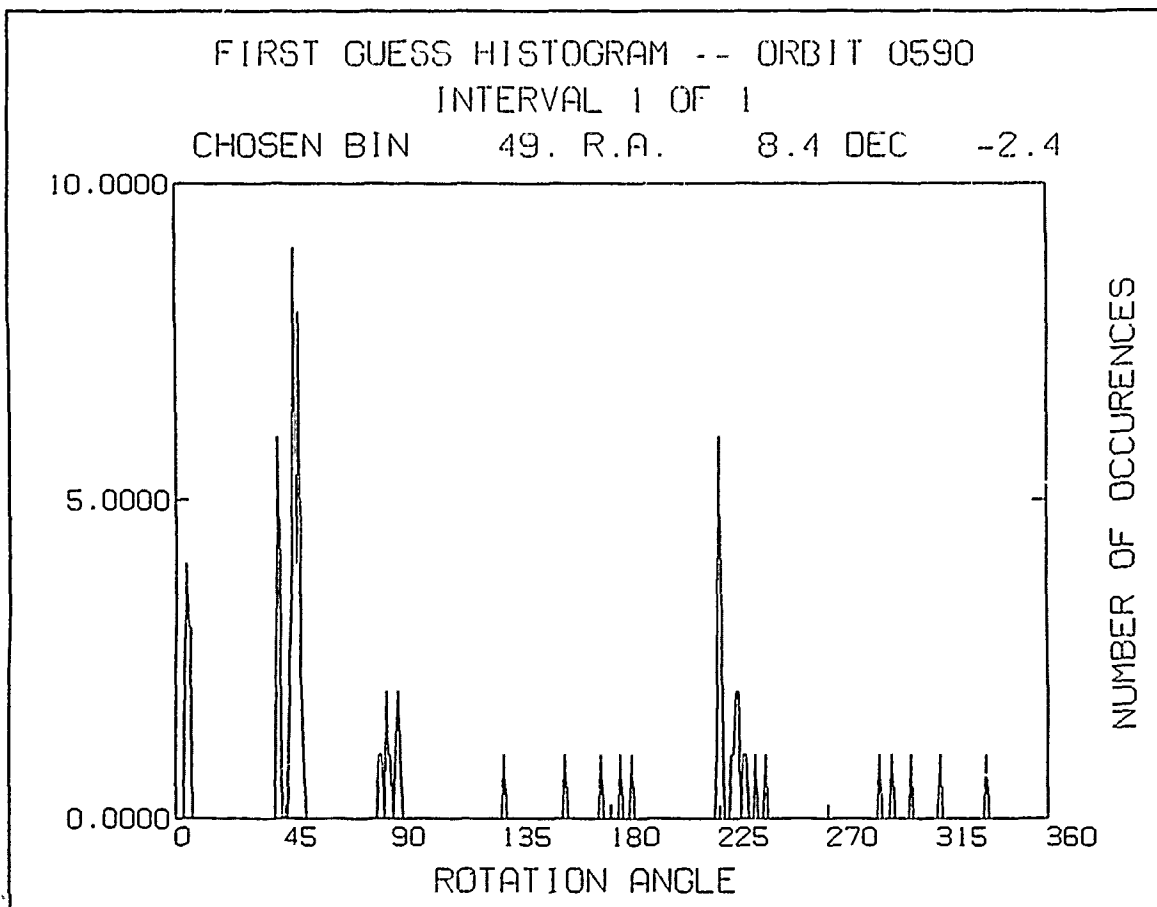
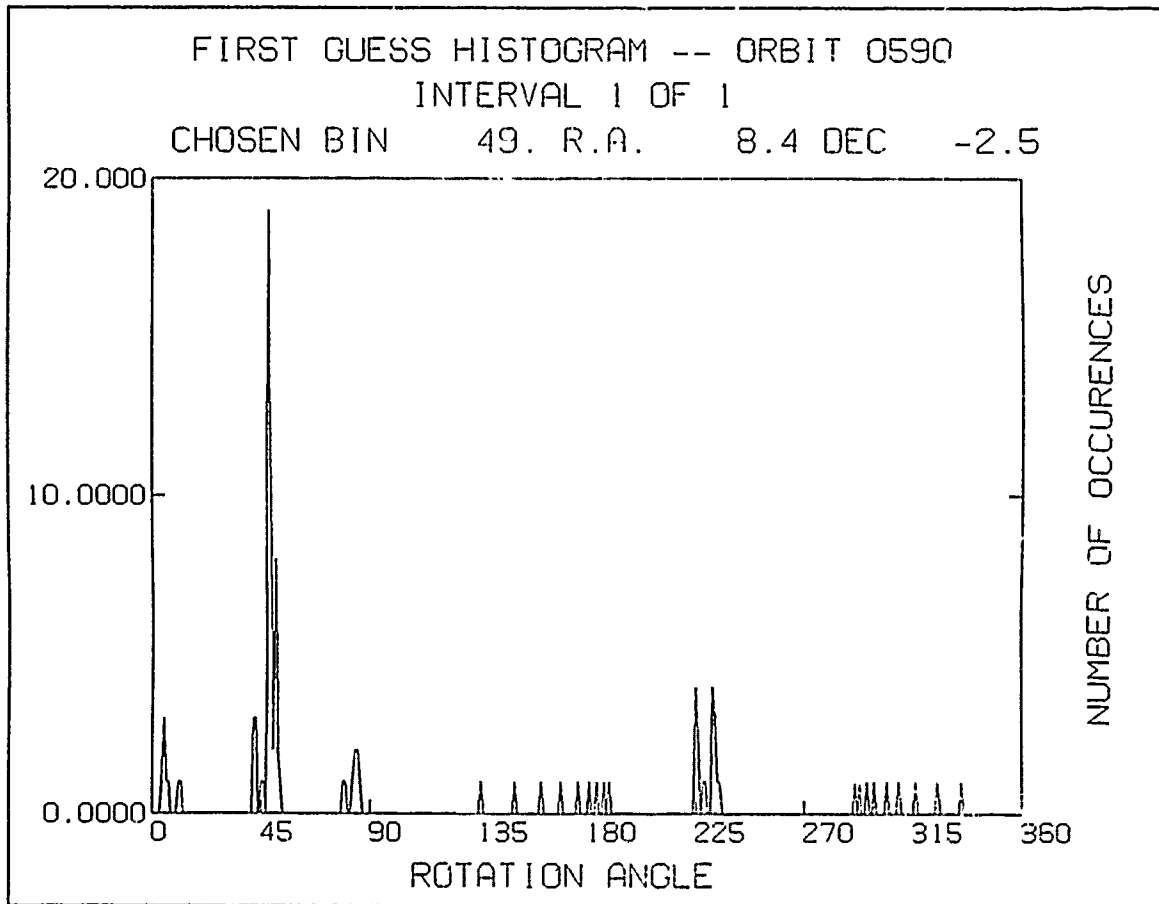


Figure 3. First guess histogram from the original CRRES Attitude Determination Program.



**Figure 4.** First guess histogram obtained by restriction of the observation sets included to those containing earth limb data.

$$Z_{ave} = w_{SS}w_{HS} \sum_{(SS/HS \text{ pairs})} Z_{SS/HS} + w_{SS}w_{Mag} \sum_{(SS/Mag \text{ pairs})} Z_{SS/Mag} \quad (3)$$

*SS/Mag Pairs.* These are calculated identically to those calculated in Section E. The solution nearest the first guess is saved for mixing with the other solutions.

*SS/HS Pairs.* There are two spin axis calculations carried out with these data for observation sets with sun sensor and horizon sensor data. They are performed in a manner similar to that described in Section E with the exception that an iterative correction is made for the earth's oblateness. First, the algorithm in Section E is performed with the spherical earth estimate for the horizon sensor to nadir angle  $\rho$ . Then, using the calculated value of  $h_1$  or  $h_2$ , the choice being deduced from selection of the proper  $z_1$  or  $z_2$ , a revised value of  $\rho$  is calculated. The algorithm for finding this value is given in Wertz (1986) pp.98-101 and will not be repeated here. The process is repeated a few times to insure convergence.

*HS/Mag Pairs.* Although there is a rather elaborate calculation of attitude from horizon sensor leading and trailing edge plus magnetometer zero crossing included in the system, this is used only when neither of the two combinations above can be found. The details of this calculation can be found in Wertz pp.366-370. This means that the calculation is used only during eclipse when earth horizon hits occur. This happens very sporadically and, as such, is not particularly useful for routine processing. Aside from this, it has been our experience that this computation almost never succeeds in producing reasonable values. This is most likely because, as we will see, the magnetic field data is not very useful beyond a few thousand kilometers altitude.

*Spin Phase Zero Time.* When the possible spin axis attitude vectors, enumerated above, have been calculated and mixed according to the weights, the time of the zero phase crossing for each observation set is calculated. At the time of zero phase, the spacecraft x-axis lies in the ECI x-y plane and is rising, by definition. This vector is given by

$$h = k \times z$$

where  $k$  is the ECI unit vector and  $z$  is the calculated spin axis vector for the observation set. The rotation angle from the sun vector  $s$  to the x-axis vector  $h$  is calculated by

$$\Phi = \Lambda(z,s,h)$$

since we know the time of the sun crossing,  $t_{SS}$  we can find the time of the zero phase crossing from

$$t_0 = t_{SS} + \Phi/\omega$$

where  $\omega$  is the spin rate. There is an equivalent calculation involving the magnetometer zero cross time that is used when the sun is not visible. Here, the model field vector  $b$  is substituted for the sun vector  $s$  and the magnetic field crossing time  $t_{mag}$  for the sun crossing time  $t_{SS}$ .

## 2.7 CADP SEGMENTATION AND FITTING

Although the attitude model produced by CADP is discarded in the present processing scheme, it is valuable to examine the details of this model in order to see why the results were not acceptable. With a set of state vectors for an orbit in hand, the CADP divides the orbit into segments. A segment occurs at the beginning and end of eclipse, at each mission event input to the program and in lieu of these, at equal intervals of predefined duration, set currently to 100 seconds. For each segment, the state vector times are normalized to the interval [-1,1] via the formula

$$X = 2 \frac{t - t_1}{t_2 - t_1} - 1 \quad (4)$$

They are then fit by standard IMSL routines [IMSL, 1987] to Chebyshev polynomials. The first few of these polynomials are

$$\begin{aligned} g_0(X) &= 1 & g_1(X) &= X \\ g_2(X) &= 2X^2 - 1 & g_3(X) &= 4X^3 - 3X \\ g_4(X) &= 8X^4 - 8X^2 \end{aligned}$$

The fitting of the right ascension  $\alpha$  and declination  $\delta$  is carried out by increasing the order of the fit until the change in the residual by increasing the order is no more than a preset parameter  $\epsilon$ . The spin rate is fit to the same polynomial expansion, however, the order is never allowed to go beyond a constant. This is necessary because the spin rate is the derivative of the spin phase, which is actually the attitude parameter of importance. This phase is evaluated by the Attitude Agency Module (AGMOD) from

$$\phi(t) = \phi_0 + \omega(X)(t-t_1)$$

where

$$\omega(x) = \omega_0 g_0(X) + \omega_1 g_1(X) + \omega_2 g_2(X)$$

Were the spin rate to change within a segment, and were the change to be modeled by even a linear term in  $\omega(X)$ , this would be incorrect since the phase is actually given by

$$\phi(t) = \phi_0 + \int_{t_1}^t \omega(t) dt \quad (5)$$

We will return to this complication, and its resolution, in the section on attitude modeling.

In any case, with a constant spin rate, the phase at the beginning of each segment is calculated in the CADP as follows. For each phase zero time, the initial phase is calculated by extrapolating backwards to the start of the segment.

$$\phi_{0,i} = -\omega(t_{0,i} - t_1)$$

These are averaged to give the value used for the phase at the start of the segment,  $\phi_0$ .

### 3. CRRES ATTITUDE CHARACTERISTICS

In order to understand the problems encountered in modeling the CRRES attitude and the reasons why the batch processed model was abandoned, it is necessary to point out some of the distinctive features of the CRRES attitude. The CRRES mission is divided into two separate classes of experiments, the Geosynchronous Transfer Orbit (GTO) experiments and the Low Altitude Satellite Studies of Ionospheric Irregularities (LASSII) experiments. The GTO phases of the mission constitute >95% of the data gathering periods. The LASSII periods are almost always less than 15 minutes in duration and present less of a problem for attitude determination. For this reason, we restrict this discussion to GTO periods, although the same general principles apply to the LASSII model. The present discussion is also restricted to attitude characteristics that are essential in the modeling. Other features will be discussed in later sections.

#### 3.1 A TYPICAL ORBIT

A plot of the attitude state vectors for Orbit 31, typical of most early orbits with eclipse, is shown in Figure 5. The plot is from the attitude quality control and fitting software developed by Radex, and consists of four panels. The top panel shows the attitude source flag, which shows the data that went into the calculation of the attitude at each point. The values taken by the source flag are the same as those given in Table 1. The next panel gives the spin axis right ascension, the next panel the declination and the bottom panel the spin rate in rpm. Concentrating first on the spin axis pointing direction, we can see that the data indicates a total of five discontinuities in the pointing direction as well as a persistent drift which seems to decrease the declination by about  $5^\circ$  at apogee.

In fact, these features of the data are not real. They result from the use of the magnetic field model and the engineering magnetometer for the calculation of attitude in periods when the resolution of the magnetometer and the accuracy of the assumed model field are not sufficient for accurate determination. One source of the discontinuities is jumping of the attitude solution between the two possible solutions for each data point. This happens when the first guess attitude, which is substantially more accurate than either of the two individual attitudes calculated from apogee magnetic field hits, falls between the two. A second source is the downlink power amplifier which causes a rather large current loop when activated, and induces a strong spacecraft magnetic field. In the absence of complicating factors, we would expect the spin axis pointing direction to be constant between attitude adjustments. There are in fact some complicating factors for CRRES, to be discussed later, but these turn out to be too small to be included

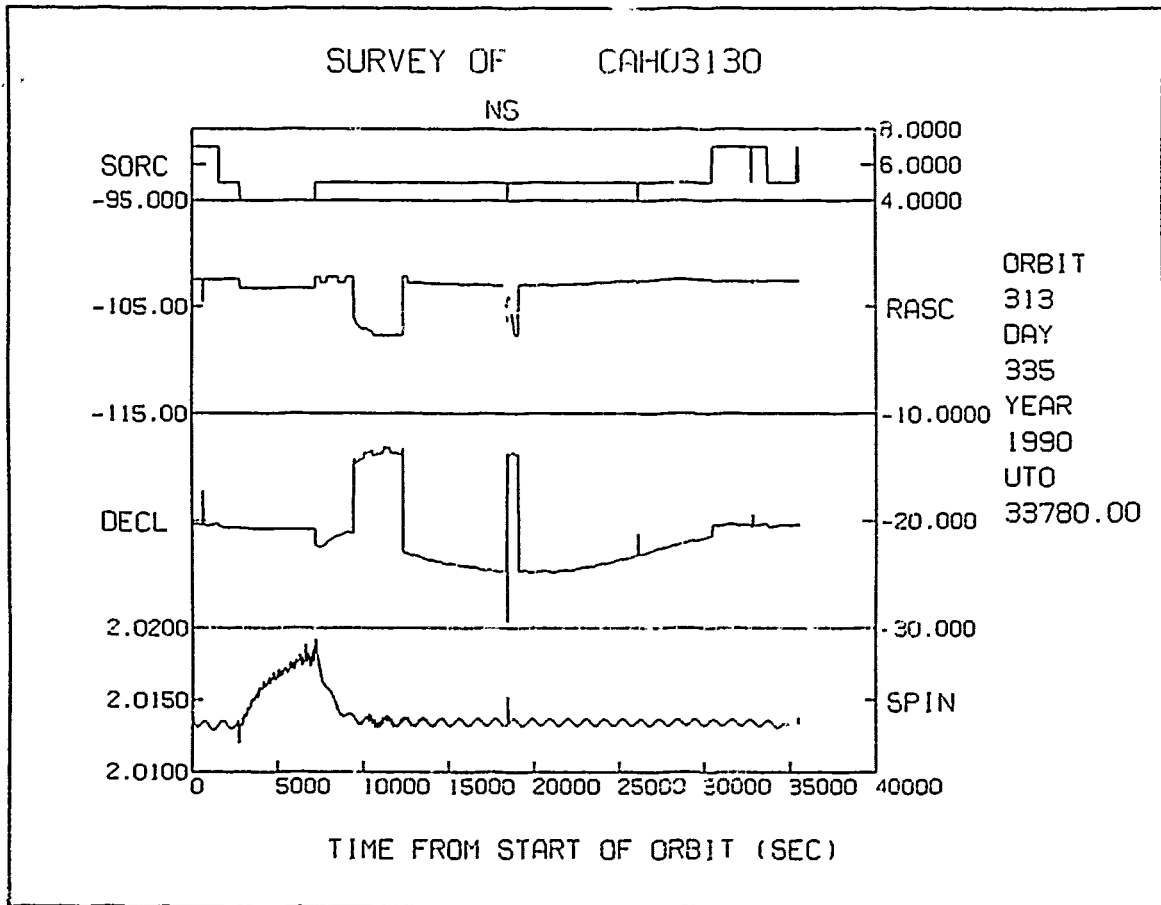


Figure 5. An attitude survey plot for Orbit 313, showing the calculated right ascension, declination and spin rate from each observation set.

in the model on a routine basis. The most accurate attitude in Figure 5 is that given by the data including earth horizon hits and sun hits (source code 7).

A second feature seen in Figure 3 is a rather dramatic increase in spin rate during eclipse (source code 4) and a more rapid decrease after the satellite emerges. This spin rate change is real and is the result, for the most part, of cooling and heating of the wire antennae. A third feature which is not so readily apparent in this orbit is a change in spin rate or spin axis pointing direction very close to both first and second perigee. Because of the interrelation between spin axis pointing direction and spin rate calculations, it is difficult to differentiate between the two for a change as small as this. The change is significant enough, though, to warrant segmentation of the near earth portions of the orbit. Comparisons with measured magnetic field have shown that this is most satisfactorily treated as a change in spin rate rather than in spin axis pointing direction.

### 3.2 CADP FIT RESULTS

Figure 6 shows an attitude quality control plot for the attitude model returned by the CADP for Orbit 313. This plot is also from the attitude modeling system and a plot such as this is produced for every orbit processed. The top three panels show the state vector values of  $\alpha$ ,  $\delta$  and  $\omega$  plotted as solid lines and the model values as dots. The bottom panel shows the phase of the sun, measured in the spacecraft frame, at the time of sun hits. Because the sun sensor is on the -x side of the spacecraft, this value should be  $180^\circ$ . The phase is calculated as follows. First, at the time of each sun hit, the instantaneous values of  $\alpha$ ,  $\delta$  and  $\omega$  are calculated. Then, the spin phase is found from

$$\phi(t_{SS}) = \phi_0 + \omega(t_{SS} - t_0) + 90^\circ$$

The  $90^\circ$  is added to make the definition of the CRRES attitude correspond to the standard rotation matrix below. The matrix  $M$  describing the instantaneous pointing directions of the spacecraft axes in ECI coordinates is given by

$$M = \begin{bmatrix} \sin \delta \sin \alpha \cos \phi - \sin \alpha \sin \phi & \sin \delta \sin \alpha \cos \phi + \cos \alpha \sin \phi & -\cos \delta \cos \phi \\ -\sin \delta \cos \alpha \sin \phi - \sin \alpha \cos \phi & -\sin \delta \sin \alpha \sin \phi + \cos \alpha \cos \phi & \cos \delta \sin \phi \\ \cos \delta \cos \alpha & \cos \delta \sin \alpha & \sin \delta \end{bmatrix} \quad (6)$$

The ECI position of the sun  $s$  is interpolated from the CRRES ephemeris then the sun vector in spacecraft coordinates is given by

$$s_{sc} = M s$$

The phase is then calculated from  $\phi_s = \tan^{-1}(s_y/s_x)$ .

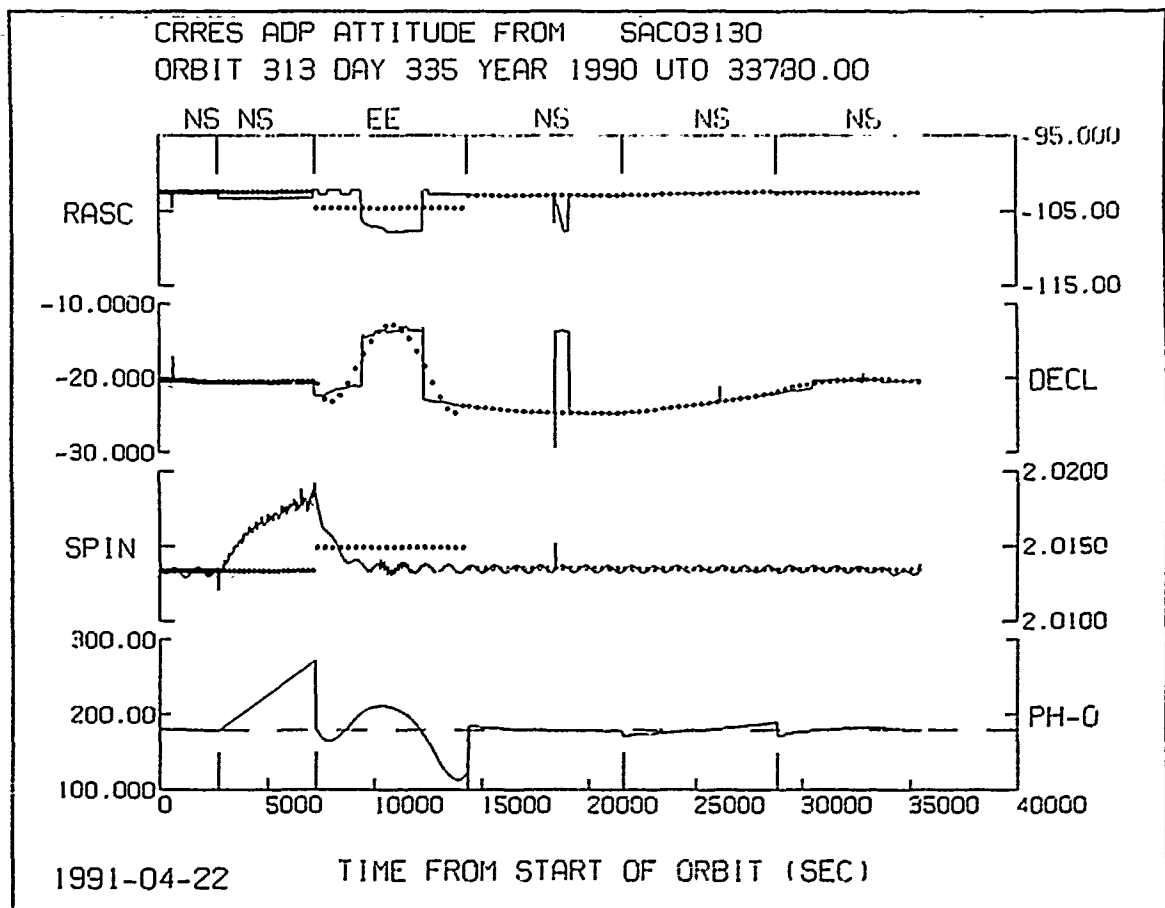


Figure 6. Quality control plot of the attitude model compared to data used for modeling for the original CADP fitting routine.

As can be seen, the CADP attitude model has several undesirable characteristics. First, the values of  $\alpha$  and  $\delta$  have been modeled as linear, quadratic and even quartic polynomials when in fact they should be nearly constant. The errors in the calculated attitude away from perigee have even been magnified by the fitting. One would prefer to use only the reliable data for modeling of  $\alpha$  and  $\delta$ . This is entirely possible since the values are constant throughout an orbit. However, this doesn't fit into the CADP modeling scheme since an independent model for  $\alpha$  and  $\delta$  is produced for each segment from data in that segment alone.

Also, during the eclipse (labeled BE) and the post-eclipse segment (EE), the spin rate has been modeled as a constant. We can see from the phase data that this results in errors of as much as one-hundred degrees in the post-eclipse segment. (Phase is not calculated for this plot during eclipse.) Clearly, a constant spin rate will not do. Finally, looking closely, we see some rather large discontinuities in phase at segment boundaries, even for sunlit intervals. This can be seen more clearly in Figure 7, which shows the angle between the magnetic field measured by the science magnetometer and the model field. The measured field requires conversion to ECI in order to calculate this angle so the angular deviation can be taken to be the combination of errors in calibration, magnetometer alignment and three-axis attitude. It also includes, of course, the difference between the actual magnetic field and the model. We will have more to say about this comparison later, but for now, it is apparent that discontinuities of 10-20° are present and that the attitude even during sunlit segments is clearly often in serious error. Discontinuities between segments of more than one-quarter degree or so can be very annoying, especially for magnetic field despinning where they cause low frequency contamination of wave spectrograms and jumps in the despin magnetic field.

### 3.3 CONSTRAINTS

Before launching into the solutions adopted, it seems a good idea to list the factors limiting the modeling effort. These are the assumptions that have been made in attacking the improvement of the model.

*The attitude must be modeled based on pure rotation.* This requirement arises for the most part from the complexity of the dynamical motion of the satellite. It was never considered practical to attempt to model nutation following attitude adjustments, if it is indeed possible. Likewise, even though it was known for some time that the wire booms would interact strongly after most attitude maneuvers, it was always considered too large a task to attempt to produce anything more than an 'averaged' attitude. Fortunately, modeling the attitude in this way allows us to obtain the required accuracy most of the time.

*Orbits must be processed independently.* Because of variability in the time it takes for tapes to arrive from different stations, it is often the case that orbits are processed out of sequence. For this reason, we can never count on being able to use data from a previous or later orbit in the modeling of attitude for any particular orbit.

*Attitude must be processed concurrently with Agency Tape Generation.* This limitation was strongest in the early orbits, when methods to deal with non-nominal behavior of the attitude were still being developed. Even later, though, when for example the length of eclipse increased so that a quadratic spin rate increase provided a more accurate representation than a linear one, some orbits were

CRRES Attitude Quality Control Plot 313 335/90 Dec 1

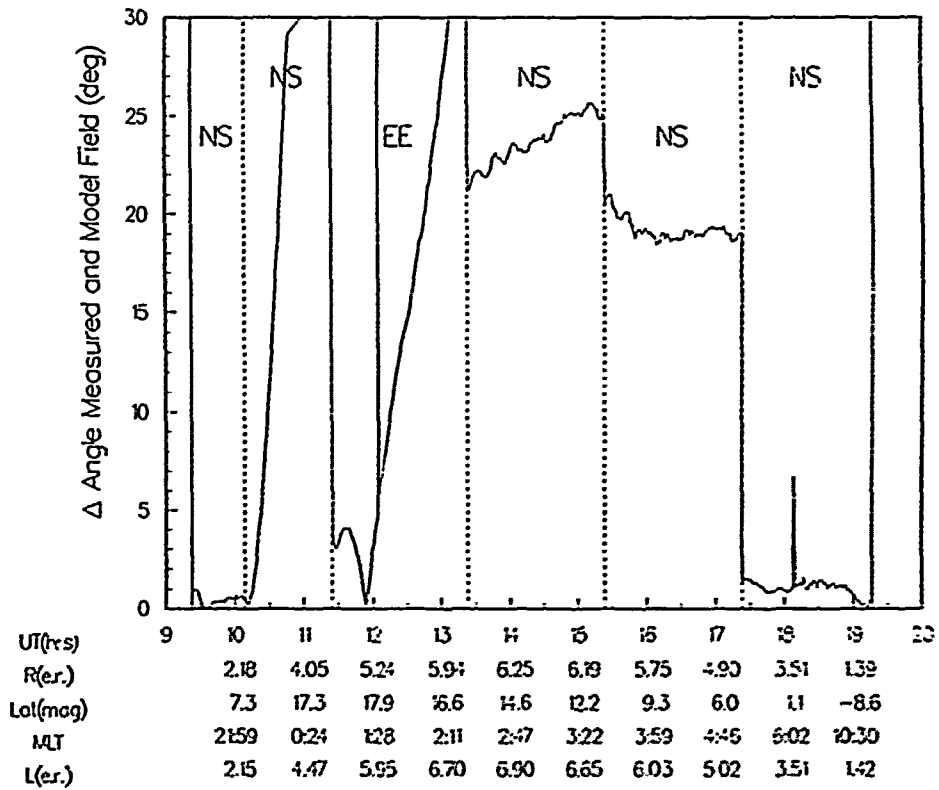


Figure 7. The angle between a model magnetic field and the field as measured by the fluxgate magnetometer. Attitude is modeled by the original CADP routine.

processed while algorithm modifications were being made which could have been better treated using the present model. This impacts the user in that he should bear in mind that all attitude is not equal and that in some instances should the Agency Tape version of the model prove inadequate, a better model may be available.

*The attitude model must be consistent with AGMOD.* In dealing with the spin rate variations, it might have been far easier to redefine the spin phase used for modeling the attitude. However, that change would have required a revision of the software subroutine AGMOD used by the agencies to evaluate the model. While this would not in all likelihood have been a disaster, and would certainly have been done if it would have enhanced the accuracy of the result, it seemed simpler to leave the structure of the model the way it was. Thus, AGMOD has only a single version.

*The attitude model must be based on data.* We have opted to avoid heuristic models in the CRRES attitude, at least so far. This pertains mostly to the modeling of the spin rate change during eclipse, since data there is limited. One reason for this limitation is that it avoids potential problems with operational changes. For example, during several orbits, some of the heaters were turned on during the eclipse. This led to a far different characteristic in the spin rate change. While the data based model used may not have been as accurate here as in unheated orbits, the use of a heuristic model would probably be wildly incorrect and might well have gone unnoticed. Another more practical reason was that in the past eclipse season, the duration of eclipses was increasing instead of decreasing and, short of a fully analytical model of spin rate change which is likely beyond our capacity, a model based on previous orbits would always have to be extrapolated.

*The attitude processing must not slow down agency tape generation.* This is a restriction in that it limits the complexity of the model. Anything we do must be successful in a majority of the cases with a minimum of intervention. Since attitude determination and modeling is nearly the final step in tape generation, the processing is done under some pressure of time. The algorithms developed must perform satisfactorily on the vast majority of orbits so as not to cause data processing to fall significantly behind.

## 4. ATTITUDE MODELING

In this section, the algorithms and features of the CRRES attitude model will be described. The modeling itself is done with a fully interactive software package, after batch processing of the attitude state vectors. The basic features of this package have been discussed before [McNeil, 1990]. The focus here will be to describe the methodology and specific algorithms that were developed to deal with the problems outlined in Section 3.

### 4.1 SPIN AXIS VECTOR

As previously pointed out, the only reliable spin axis data comes from periods of the orbit with both sun and earth limb contacts. We also claimed that the spin axis pointing direction was constant during an orbit in the absence of an attitude adjustment. This is not precisely true. From a survey of a large number of orbits around Orbit 250, we have found that the spin axis attitude does indeed change by something on the order of  $0.05^\circ$  per orbit. There are two reasons for ignoring this change. First, the change is too small to be detected reliably within a single orbit since the maximum resolution is around  $0.5^\circ$  mainly on account of the sun sensor. Since we are required to process each orbit independently, incorporation of this small change into the modeling would be impossible. Also, it seems likely that this change is due to a gravity gradient and/or atmospheric drag near perigee. If so, then the change occurs over a rather short period of time very near perigee and the attitude would be expected to be quite constant throughout the greater part of the orbit. We find that a constant spin axis pointing direction is adequate.

*Normal Orbits.* A typical GTO orbit will have two to three periods of earth horizon data. The number and duration of these depends on the orientation of perigee with respect to the sun. To calculate the averaged values of  $\alpha$  and  $\delta$  in an orbit, a global fit is done on the values for all state vectors weighing very heavily the data from sun plus earth observation sets. These values are used in all segments of the orbit. We have not, to date, encountered an orbit without earth data, even when periods of data are missing due to missing tapes. Should CRRES go to partial data coverage because of, for example, failure of one of the tape recorders, this possibility might well have to be addressed. One solution would be to relax the requirement against using data from successive orbits. Since the change in pointing direction is quite small from orbit to orbit, values from a previous orbit could be used without degrading the accuracy of the solution.

*Attitude Adjustments.* In orbits with attitude adjustments, a global average of  $\alpha$  and  $\delta$  is calculated with data both before and after the adjustment. For these, the modeled pointing direction changes discontinuously at the beginning of the first adjustment segment. For a few orbits missing first perigee earth hits and containing attitude adjustments early on in the orbit, the lack of pre-adjust data presented a problem. For these cases, sun plus magnetic field data very near first perigee was used to calculate the pre-adjust attitude. The attitude result from the sun and magnetometer within a couple of thousand kilometers of perigee is virtually indistinguishable from that calculated with earth data anyway.

## 4.2 SPIN RATE

In that the instantaneous spin phase in the model is calculated from an initial phase and the spin rate, the modeling of spin rate and spin phase are interchangeable. As noted previously, one severe limitation of the original attitude model was that the spin rate had to be constant within a segment. Another problem, not readily apparent in Figure 6, was that the spin phase zero time for each observation set was calculated using the spin axis pointing direction for that observation set. We have seen that the vast majority of these are in error by several degrees. This error would be propagated into and is in fact magnified in the phase zero times used to model the phase if they were not corrected.

The first step in modeling the phase is to use the global averaged right ascension and declination determined from earth sensor periods to calculate a new set of phase zero times from the time of each observation set containing sun data. The time assigned to each observation set is also the time of the sun hit. Observation sets without sun, *i.e.* during eclipse, are treated below. The calculation of a new set of phase zero times,  $t_{0,i}$  goes precisely as described in Section 2.7 with the global average  $z$  replacing the observation set  $z$  used in the CADP.

Next, these phase zero times are used to calculate a phase variable as follows. An averaged *constant* spin rate  $\omega_a$  is calculated over the segment. Then the phase zero times are used to calculate

$$\phi_i = \omega_a(t_{0,i} - t_1)$$

These are modulated by  $2\pi$  and corrected should the value pass  $2\pi$  on successive points. Since the  $\phi_i$ 's represent the phase plus the initial phase at the time of phase zero, if a plot of  $\phi_i$  against  $t_{0,i}$  is constant, then  $\omega_a$  is the true spin rate and

$$\phi_0 = -\phi_i$$

Since  $\phi$  is the integral of  $\omega$ , the determination of phase from phase data instead of from spin rate data seems likely to be more accurate than the calculation of phase from a set of successive measured spin rates. From the variation in the  $\phi_i$  values, constant through quadratic correction terms to the spin rate are determined. Since  $\omega$  is a derivative, this means that the model allows for up to cubic variation in the phase during a segment.

For no particular reason save convenience, the determination of the correction terms is done by fitting  $\phi_i$  with the same Chebyshev polynomials as were used for  $\alpha$  and  $\delta$ . We then can obtain the phase at any point  $X$  from

$$\phi(X) = 6\omega_A\tau + \pi_0 + \pi_1 X + \pi_2[2X^2 - 1] + \pi_3[4X^3 - 3X] \quad (7)$$

where the  $\pi_i$  are the expansion coefficients. Evaluation of the phase by the attitude model, however, requires the expansion of the spin rate as follows

$$\phi(\tau) = \phi_0 + 6\tau(\omega_0 + \omega_1 X + \omega_2[2X^2 - 1]) \quad (8)$$

where  $\tau = t - t_1$ . When evaluated in terms of  $\tau$ , this gives

$$\phi(\tau) = \phi_0 + 6(\omega_0 - \omega_1 + \omega_2)\tau + 6(2\omega_1 - 8\omega_2)\frac{\tau^2}{\Delta} + 6 \cdot 8\omega_2\frac{\tau^3}{\Delta^2} \quad (9)$$

where  $\Delta = t_2 - t_1$ . As may be seen, it would have been substantially easier to expand the phase, modulated by the average spin rate, in Chebyshev coefficients in the modeling. Since the agency module expands the spin rate, however, we must determine the coefficients  $\omega_1$  from the measured coefficients  $\pi_1$ . Before doing so, though, we must note one complication. Because the quantity fit by the Chebyshev expansion is actually the value required to obtain zero phase at each fit time, the true phase is given by

$$\phi(X) = 6\omega_A \tau - \pi_0 - \pi_1 X - \pi_2[2X^2 - 1] - \pi_3[4X^3 - 3X] \quad (10)$$

First, evaluating the Eq(10) at  $\tau=0$  and  $X=-1$ , we find

$$\phi_0 = -\pi_0 + \pi_1 - \pi_2 + \pi_3 \quad (11)$$

Next, we evaluate Eq(7) and Eq(9) at  $\tau=0.25\Delta$  and  $X=-0.5$  to give

$$3\omega_A \Delta - \pi_1 + 3\pi_2 - 4\pi_3 = 6\Delta\left(\frac{\omega_0}{2} - \frac{\omega_1}{4} - \frac{\omega_2}{4}\right) \quad (12)$$

In the same way, evaluation at  $\tau=\Delta$  and  $X=1$  gives

$$6\omega_A \Delta - 2\pi_1 - 2\pi_3 = 6\Delta(\omega_0 + \omega_1 + \omega_2) \quad (13)$$

and evaluation at  $t=\Delta/2$  and  $X=0$  gives

$$3\omega_A \Delta - \pi_1 + 2\pi_2 - \pi_3 = 6\Delta\left(\frac{\omega_0}{2} - \frac{\omega_2}{2}\right) \quad (14)$$

Taking 4 times Eq(12) gives

$$12\omega_A \Delta - 4\pi_1 + 12\pi_2 - 16\pi_3 = 6\Delta(2\omega_0 - \omega_1 - \omega_2) \quad (15)$$

Adding this to Eq(13) we find

$$\omega_0 = \frac{18\omega_A\Delta - 6\pi_1 - 4\pi_2 - 18\pi_3}{18\Delta} \quad (16)$$

Next, from Eq(14) we find

$$\omega_2 = \omega_0 - \frac{6\omega_A\Delta - 2\pi_1 + 4\pi_2 - 2\pi_3}{6\Delta} \quad (17)$$

and from Eq(13) we find

$$\omega_1 = -\omega_0 - \omega_2 + \frac{6\omega_A\Delta - 2\pi_1 - 2\pi_3}{6\Delta} \quad (18)$$

### 4.3 ECLIPSE MODEL

During the eclipse, the only information of any practical use is the spin rate measured by the time between the zero crossings of the x-axis and the magnetic field. To model the spin rate increase during eclipse, we perform a fit to the spin rate using the Chebyshev expansion. We then use characteristics of this fit to model the phase.

Assume that a quadratic fit of  $\omega$  during the eclipse results in coefficients  $\sigma_0$ ,  $\sigma_1$  and  $\sigma_2$ . We use the first and second derivatives of the measured  $\omega(t)$  for the first and second derivatives of the spin rate in the model. These, as with the previous correction terms, require modification because of the way in which phase is evaluated by AGMOD. The resulting coefficients are

$$\omega_1 = \sigma_1 - 4\sigma_2/6$$

$$\omega_2 = \sigma_2/3$$

We match the phase at the start of the eclipse segment to the phase at the end of the previous segment. We modify the constant term in the spin rate according to

$$\omega_0 = \omega_c - \sigma_0 - \sigma_1$$

where  $\omega_c$  is a correction term to make the phase at the end of the eclipse segment match the phase at the beginning of the next segment, calculated as follows. If  $\alpha$  is the number of 'excess' revolutions in the segment calculated from the difference between

$$\phi(t_2) = \phi_0 + (\sigma_0 + \sigma_1)(t_2 - t_1)$$

and the phase at the beginning of the next segment, then

$$\omega_c = 60\alpha/(t_2 - t_1)$$

with  $\omega$ , as usual, in rpm.

Finally, because the segment following the eclipse is very short and because wire boom motion, to be discussed later, often confounds the calculations somewhat in this area, the phase at the end of the post-eclipse segment (EE) is matched to that at the beginning of the next segment by modification of the constant term in the spin rate. This is done in the same way as in the previous calculation.

We should mention one further point concerning the transformation of spin rate to phase. Because the spin rate expansions in Sections 4.2 and 4.3 consist of terms which will give the correct of the phase instead of the spin rate, evaluation of the Chebyshev expansion with these coefficients will not give the correct spin rate. The expression for the instantaneous spin rate using the spin rate coefficients is

$$\omega(\Delta) = \omega_0 - \omega_1 + \omega_2 + (4\omega_1 - 16\omega_2)\Delta + 24\omega_2\Delta^2$$

where

$$\Delta = (t - t_1)/(t_2 - t_1)$$

This is of no practical use unless one wants to calculate the instantaneous spin rate given by the attitude model, as we do in the survey plots.

#### 4.4 SEGMENTATION

Because of the incorporation of the spin rate correction terms based on phase fitting into the modeled spin rate, it is possible to increase the duration of segments, at least in those periods for which a quadratic spin rate is a good approximation. This has the advantage of reducing the number of discontinuities in an orbit. The modeling software automatically segments normal orbits with a single segment up to eclipse time (if there is one), and two to three segments after eclipse. This is to provide an adequate representation of the spin rate decrease after emergence from eclipse. In every orbit small segments are placed before and after perigee, unless this time comes during eclipse. This is to allow for more accurate modeling of what appears to be a spin rate change at perigee. Also, segments are placed interactively where mission events or anomalies occur. A survey of these anomalies is given in Section 5.

We should emphasize that the segmentation varies depending on the characteristics of a particular orbit. Several orbits prior to Orbit 300 were processed with two post-eclipse segments and a linear variation of the spin rate in eclipse. This does not mean that they are substantially less accurate, however, since the shorter eclipses gave smaller spin rate changes and required fewer segments.

By orbit 425, eclipse had disappeared and orbits without anomalies of other sorts were treated with two one-hour segments at either end and a single segment for the remainder. When eclipse came back again, around orbit 595, the old eclipse model was used for a while. Then, post-eclipse segments were modified or removed when eclipse slipped nearer second perigee. By orbit 800, subtle changes in the spin rate behavior forced the addition of a quadratic term to the spin rate in sunlit periods.

This rather rough history of the chosen segmentation is intended to show that the attitude model is anything but static, the characteristics dependant to a large extent on the judgment of the attitude analyst, within the constraints of the specified tolerable error level and other constraints enumerated previously. Schemes are modified when it becomes apparent that the current method is becoming inadequate and when reasonable changes will lead to a significantly better result.

#### 4.5 RESULTS

Figure 8 shows an attitude quality control plot for the model calculated as described above. The corresponding plot of the angular deviation of the measured and model field is shown in Figure 9. As should be apparent from Figure 8, the attitude model reproduces the data quite well, with the exception of  $\alpha$  and  $\delta$  at off-perigee times. As we know, the calculated values of  $\alpha$  and  $\delta$  are incorrect except when there are earth hits and very near perigee, where the modeled values intercept the data as they should. The modeled spin rate follows the calculated one quite well and the phase calculation indicates that the model phase is consistent with the data to within one-half degree at most. The 19 minute oscillation in the values of the sun phase, given in the bottom panel, arise from the oscillations of the wire booms. Since the sun is high in the spacecraft frame, the actual motion of the spin axis is substantially less than would be indicated by the magnitude of this oscillation.

Turning to the magnetic field plot, shown in Figure 9, we see that the angular deviation between measured and model field is less than about  $2^\circ$  throughout the orbit. This orbit is fairly typical as far as attitude determination is concerned but is somewhat unique in that magnetic field is unusually quiet, leading to good agreement between the measurements and the model field, which is IGRF85 extrapolated to date plus Olson-Pfitzer77 Quiet External Field Model. As mentioned, the angular deviation between measured and model field has components arising from magnetometer calibration and alignment, true discrepancy between the model and actual field and attitude errors. Had we chosen a more disturbed period, we might see something like Figure 10. There, the agreement is still less than  $2^\circ$  near perigee, but deviates by several degrees once the external magnetic field comes into play. These deviations underscore the fact that magnetic field based attitude calculation is of little use more than a few thousand kilometers from the earth. The attitude modeling does not suffer from this limitation because we have chosen to rely on sun and earth sensor data for attitude calculation.

In spite of the large deviations caused by the inadequacy of the model field, we can still use this plot to evaluate the soundness of the attitude throughout the entire orbit. First, we note that the spin axis pointing direction is the same throughout the orbit and the phase, based on timing of sun hits, should be equally accurate in all sunlit segments. Thus, the attitude points near apogee should be of the same level of precision as those at perigee. Next, we note that the attitude is continuous throughout a segment but generally discontinuous at the boundaries. Because of the general trend of the deviation from segment 2 until 10:20 when the waves are encountered, we can be safe in mentally subtracting out what

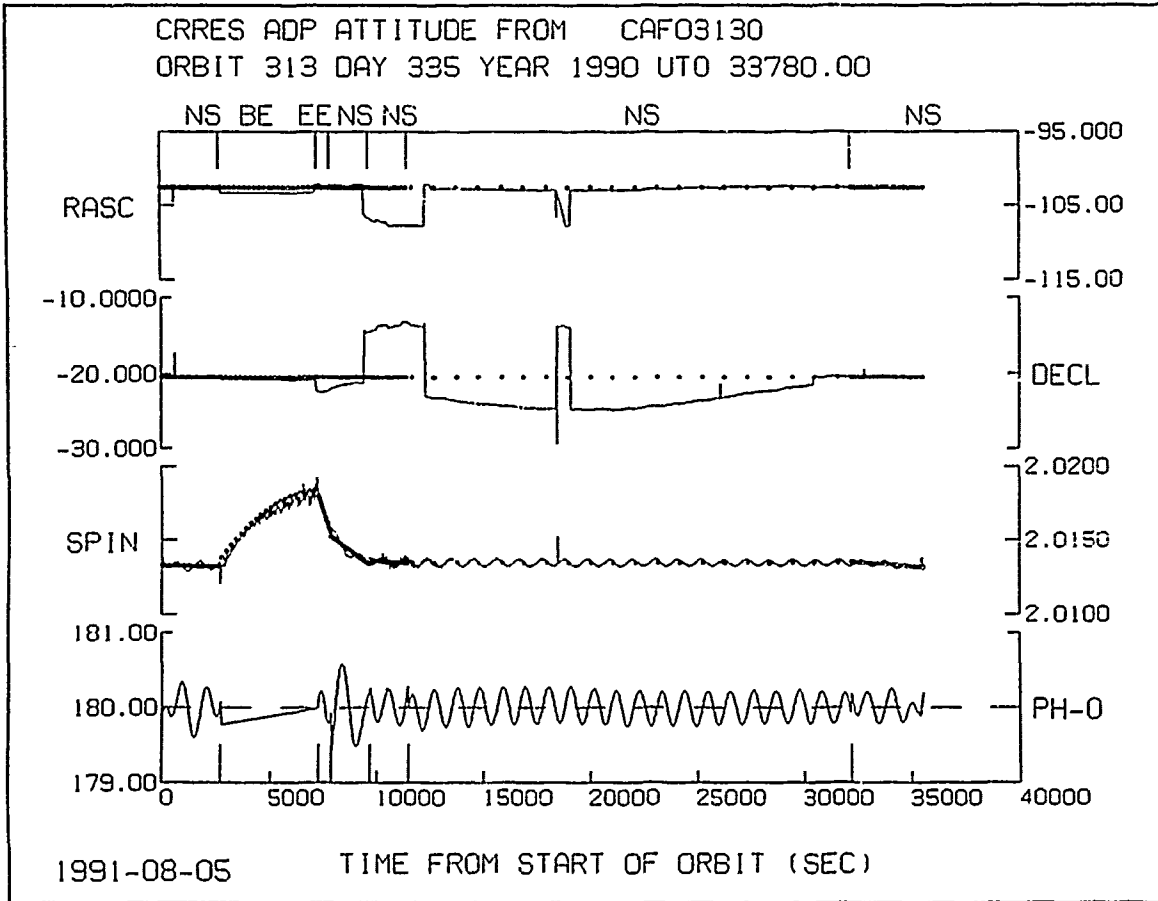


**Figure 8.** Same as Figure 6 but using the model generated by the present attitude modeling software.

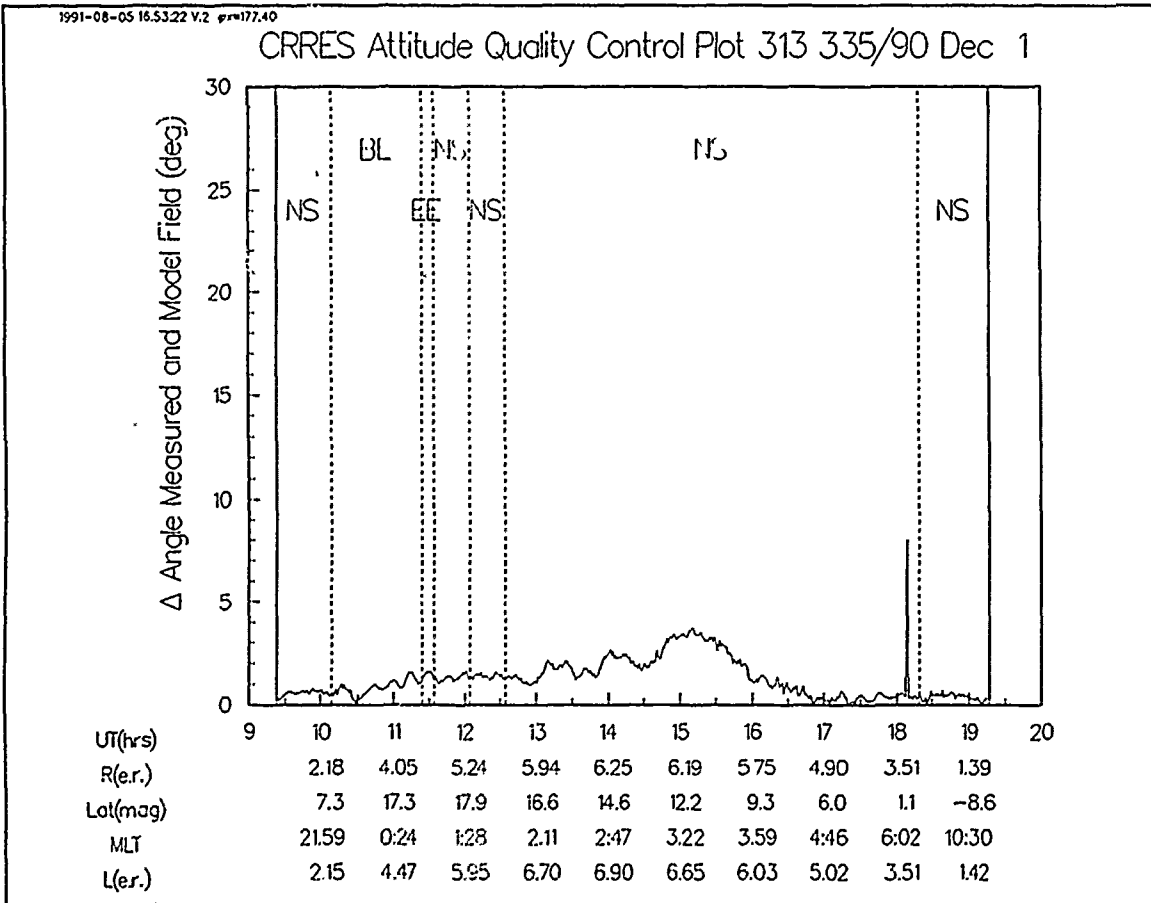
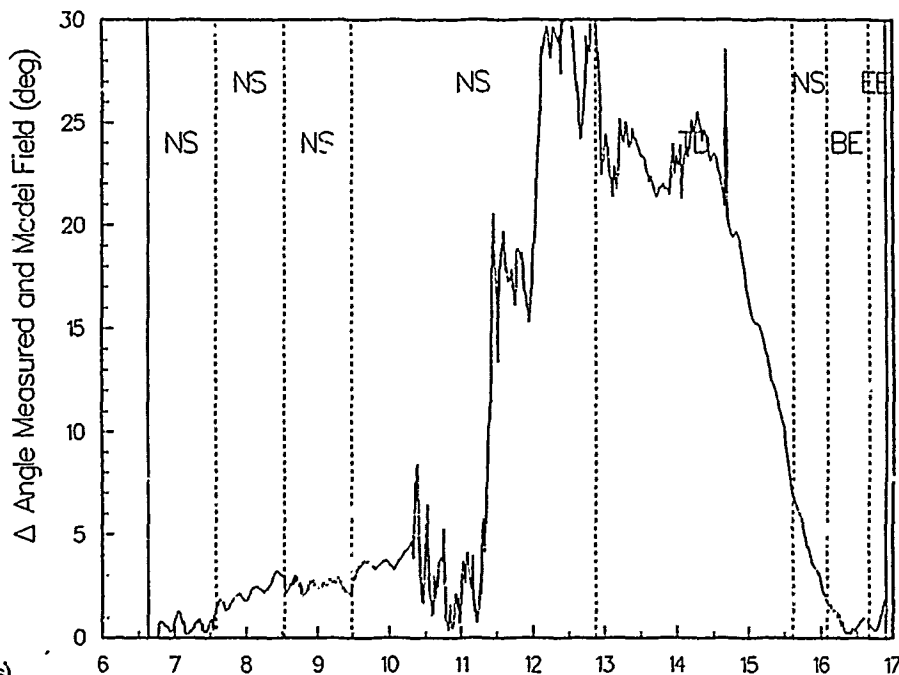


**Figure 9.** Same as Figure 5, but with the attitude model generated by the current attitude modeling software.

1991-08-13 10:43:17 V2 #1=177.40

CRRES Attitude Quality Control Plot 795 168/91 Jun 17



UT(hrs)	6	7	8	9	10	11	12	13	14	15	16	17
R(er.)		1.60	3.68	3.74	5.89	6.34	6.43	6.17	5.54	4.47	2.79	
Lat(mag)		-5.4	-23.5	-26.7	-28.0	-28.5	-28.4	-27.8	-26.6	-24.4	-18.8	
MLT		11:38	15:12	16:21	17:08	17:43	18:15	18:51	19:34	20:35	22:31	
L(er.)		155	4.34	6.36	7.59	8.21	8.35	8.00	7.09	5.50	3.04	

Figure 10. Angular deviation between measured and model field during a disturbed period.

is likely a natural deviation. Another factor reinforcing this is that the maximum errors in a segment should come at the segment boundaries. Since the segments are fit independently, the level of discontinuity at the boundaries is a measure of the maximum error expected. Here discontinuities are all less than one degree. The good match between the segment beginning at 13:00 and the one at 15:30 indicates as well that the attitude during these periods is probably no worse than it is at perigee. During the BE and EE segments, we can once again rely on the actual value of the deviation since model and measured field are expected to agree well here.

## 5. ERROR ESTIMATES

In this section, estimates are given for the expected level of accuracy of the CRRES attitude model. Accuracy is judged mainly from plots like Figures 9 and 10 of the angle between the magnetic field measured by the science magnetometer and the IGRF85 model field. The calibration and alignment of the magnetometer is therefore crucial in this comparison. The elevations and relative phase angles of the magnetometer axes are measured routinely during on-orbit calibration. However, the absolute phase of the instrument is somewhat in question due to mis-deployment of the magnetometer boom. The value chosen here,  $177.4^\circ$ , was calculated by minimization of the angular deviation of the measured and model field in the first hour after perigee over the course of many orbits. Variation of this angle would more or less lead to the addition of an equivalent angular error to these plots. The important point to bear in mind is that the magnetometer calibrations and alignments are the same for each plot. Barring some systematic error, *e.g.* the relative timing of attitude and magnetometer signals (this has in fact been ruled out on other grounds) these plots should provide reliable error estimates.

### 5.1 NOMINAL ORBITS

The vast majority of the magnetic field plots show deviations like those of Figure 9 or 10. From this, we conclude that the accuracy of the vast majority of CRRES attitude is around  $1-2^\circ$ . Exceptions to this arise most commonly following attitude adjustments. For these orbits and a few following them, errors in certain regions exceed this level. These will be discussed in detail below.

### 5.2 ATTITUDE ADJUST ORBITS

Attitude adjustments are made to keep the satellite spin axis between  $5$  and  $15^\circ$  of sun pointing. Problems arise following the adjustment because of two types of motion. Nutation of the spacecraft makes it difficult in some cases to accurately calculate the phase after the maneuver. Also, a very strong interaction of the spacecraft with the wire antennae causes a long period oscillation in the calculated phase. This makes for difficult modeling of periods when the spacecraft experiences actual spin rate changes.

Since the attitude model for CRRES is an 'averaged' model, meaning that it does not attempt to include short duration periodic motion such as nutation, we must first examine the magnitude of such motion following attitude adjustment before evaluation of the 'error' in the model itself. Figure 11 shows the measured angle between the sun and the spacecraft spin axis during and after an attitude adjustment.

We see nutation of as much as  $10^\circ$  immediately after the adjustment, about three-quarters the way through Orbit 619. By the beginning of Orbit 620, this has damped to approximately  $5^\circ$  and is about  $3^\circ$  by the beginning of Orbit 621. In what follows, then, we must keep in mind that the errors shown in the magnetic field plots represent a combination of errors in the averaged attitude, which is the attitude modeled, and true short term oscillation of the spacecraft attitude.

Figures 12 through 14 show a typical attitude adjustment and two orbits following it. The adjustment itself takes place in Orbit 802. This orbit is further complicated by three clock jumps (TD), one about two hours after the maneuver. From the magnitude of the discontinuity at the beginning of the maneuver segment (AA) and from the general behavior of the magnetic field before the maneuver it would seem that the attitude immediately after the adjust is not at all bad, perhaps in error by  $5^\circ$  or so. At the TD segment, though, there is a discontinuity of almost  $20^\circ$ . Clock jumps, discussed more fully in Section V, might be expected to give rise to no discontinuity when properly processed and compared to a geophysical requiring attitude for the comparison. However, the wire boom motion immediately following the maneuver has probably led to improper fitting of the phase near the segment boundaries. This happens when the polynomial fitting algorithm mistakes a partial oscillation near segment ends for a true spin rate change. The smaller the segment the more intense this effect will be since partial cycles of the 19 minute oscillation will constitute a greater portion of the whole. The same effect can be seen in the first TD segment, which has discontinuities in the  $2-3^\circ$  range. There, the segment was extremely short due to a second clock jump. The oscillations present there were remnants of another attitude adjust some two orbits prior to this one. Again from the looks of the overall variation of the field, we must admit to an approximately  $10^\circ$  error near the beginning of the third TD segment. We should emphasize that most attitude adjusts do not contain discontinuities of this magnitude. In the usual case, a segment would not be put in so soon after the maneuver.

Moving on to the BE segment, we can see again the 'end effects' of the wire boom motion leading to errors in the phase near the segment boundaries. As discussed in the modeling section, the phase at the beginning of the BE segment is matched to the end of the previous segment then the spin rate is adjusted to match the phase at the beginning of the EE segment. This means that the error from fitting the third TD segment is carried over to the beginning of the BE segment. Since the same 'end effects' are present in the EE segment, especially severe here because the segment is so short, the beginning and end phase there is also in error by as much as  $10^\circ$ . Of this, perhaps one-half is actual motion of the spacecraft that deviates from the average model sought. This case is one of the most severe, due to the very short EE segment and due to the presence of the clock jump. However, it serves the purpose in demonstrating that dynamical motion of the spacecraft make attitude modeling extremely difficult after an attitude adjustment. We cannot increase the segment durations due to eclipses, clock jumps and simply the end of the orbit. Nor, however, can we accurately ascertain the spin rate changes because of the large amplitude oscillations that appear due to wire boom interactions. Fortunately, this interaction dampens quite rapidly, as we will see shortly.

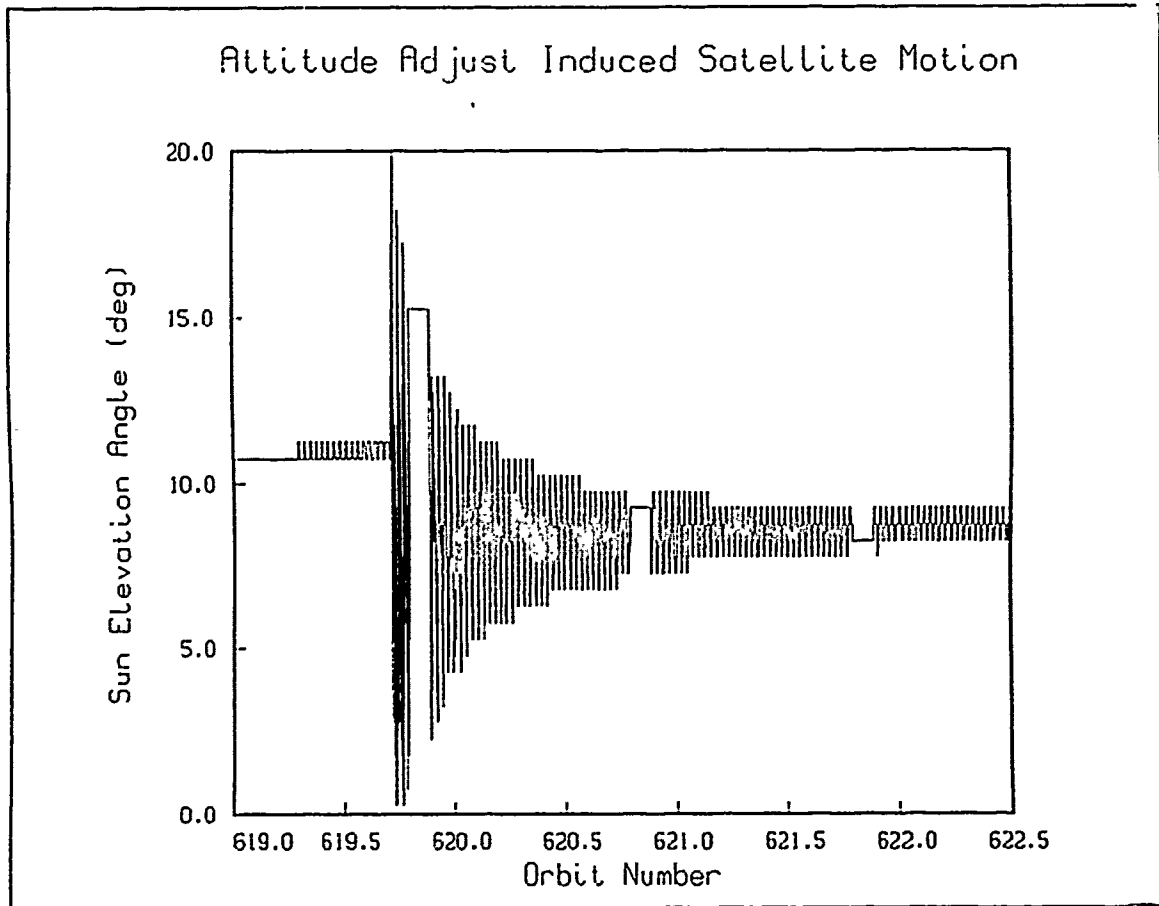
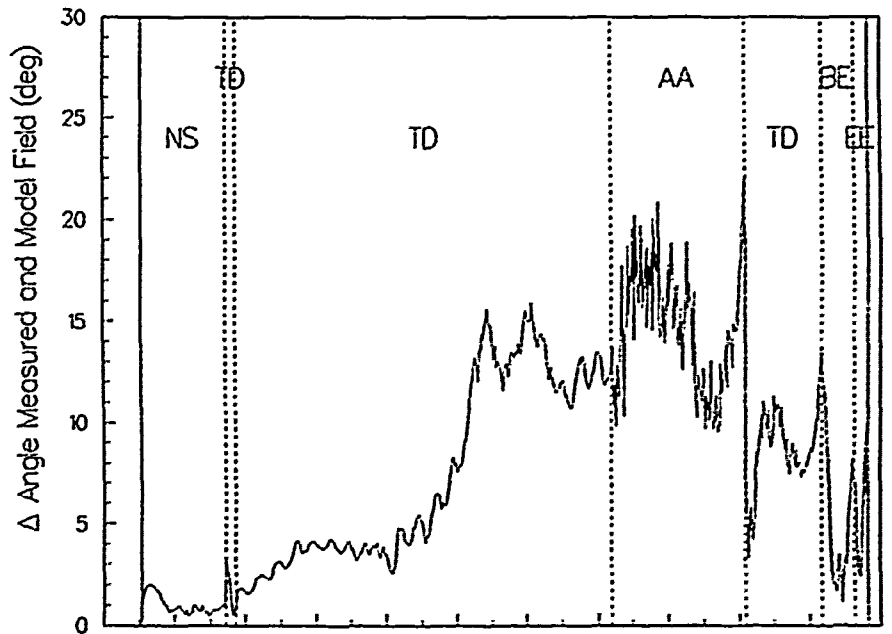


Figure 11. Angle between the spin axis and the sun.

1991-08-13 10:52:43 V.2 #3=07.40

CRRES Attitude Quality Control Plot 820 178/91 Jun 27



UT(hrs)	22	23	24	25	26	27	28	29	30	31	32	33
R(er.)		1.83	3.85	5.15	5.95	6.38	6.44	6.16	5.50	4.39	2.67	
Lat(deg)		-3.4	-9.6	-11.4	-12.7	-13.7	-14.4	-14.8	-14.3	-11.8	-2.1	
MLT		12:20	15:27	16:36	17:20	17:55	18:27	18:59	19:36	20:28	22:09	
L(er.)		1.81	4.01	5.46	6.35	6.81	6.93	6.70	6.02	4.72	2.67	

Figure 12. Angular deviation plot for an orbit containing an attitude adjustment.

1991-08-13 11:04:50 V.2 sp=177.40

CRRES Attitude Quality Control Plot 821 179/91 Jun 28

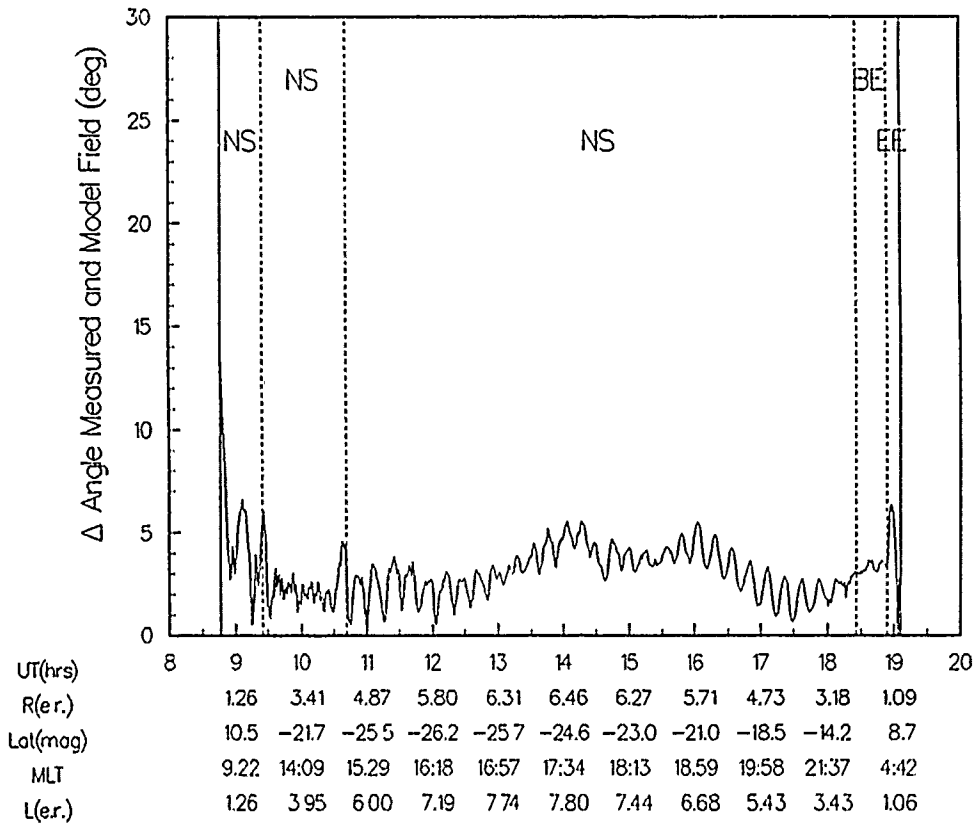


Figure 13. Angular deviation plot for one orbit after an attitude adjustment.

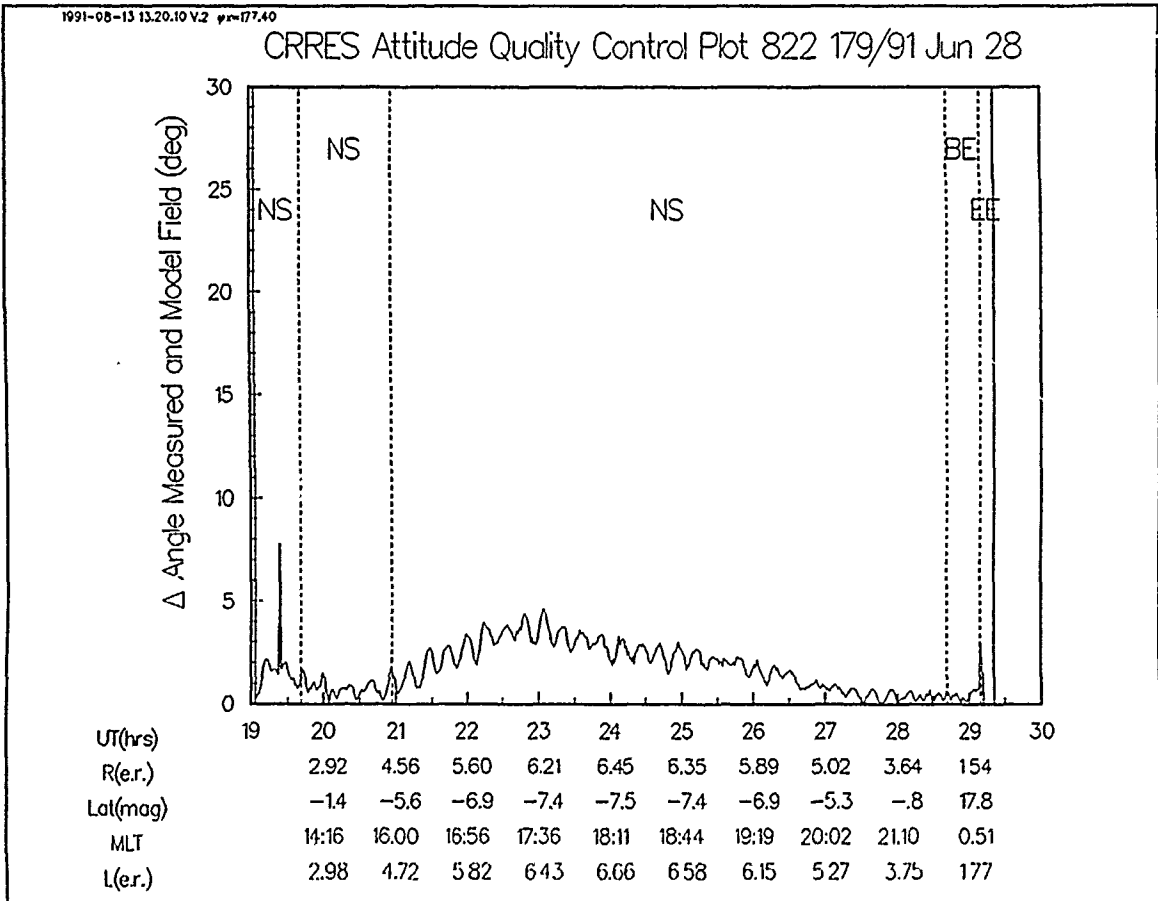


Figure 14. Angular deviation plot two orbits after an attitude adjustment.

Figure 13 shows the orbit following the attitude adjustment under consideration. First, note that the magnitude of the wire boom motion, seen most clearly around 11:30, is still around  $4^\circ$ . Next, recall that in the first segment, we are trying to model a relatively rapid spin rate decrease due to emergence from eclipse just prior to perigee. We see that in the first segment, the wire boom motion has confounded the fitting of the phase somewhat, leading to an initial deviation of  $10^\circ$ . We remember again, though, that the spacecraft attitude is experiencing a complex 19 minute oscillation of perhaps  $5^\circ$  at this point. This rapidly drops below the  $5^\circ$  level, though, at least on average when the actual motion of the spacecraft is discounted. In segment 2, we see errors of approximately  $3^\circ$  and those in segment 3 are probably no larger. The eclipse as well shows no particular changes indicating increased error. In the final EE segment, however, we see again that wire boom interaction has been translated into spin rate changes in the model and deviations of perhaps as much as  $5^\circ$  are present in this segment. This is due mostly to the 'end effects' since actual non-nominal motion is down to about the  $1^\circ$  level at this point.

Finally, we show in Figure 14 the next orbit, beginning about one and one-half orbits after the adjustment. We see that the errors in the first segment are below the  $2^\circ$  level and those in the remainder are even smaller, near  $1^\circ$ . Unfortunately, the EE segment in this plot is empty due to a switch to LASSII mode and consequent loss of the science magnetometer data. Other orbits, however, show that this error is less than  $2^\circ$  as well.

### 5.3 OTHER ANOMALIES

Errors arising in the calculation and modeling of the attitude during other periods of non-nominal behavior are not particularly severe. This is for the most part because the wire boom interaction resulting from such things as spin rate adjustments or canister ejections is relatively high frequency and does not interfere with spin rate modeling. The modeling produces an averaged attitude as desired without contamination from boom interactions. The only aspect that might be of concern with other types of anomalies is the precise timing of these events. At the time of attitude processing, there are some problems inherent in the determination of the precise times of attitude events. Pass plans are often incomplete and mission event reports are often not available. Consequently, in order to keep pace with processing, the times for all unusual attitude events and the segmentation of the attitude model accordingly are obtained from inspection of the attitude data itself. This pertains to attitude adjustments, spin rate changes and canister releases, as well as the timing discontinuities discussed above. The most sensitive measure of the first three of these is the calculated spin rate, available only at the spin frequency, since it is extremely sensitive to variations in phase and spin axis direction. This means that the segmentation of orbits around events is accurate only to one minute or so. As a consequence, maneuvers that cause a change in the spin rate may result in attitude models with phase errors of a few degrees within a minute of the exact maneuver time. In special cases where the data immediately surrounding an attitude maneuver is critical, more precise segment boundaries can be incorporated into the model and a revised set of model coefficients issued on an individual bases. This has been done, for example, for photometer analysis following the canister releases.

## 5.4 SUMMARY

The above examples present what we believe to be an honest assessment of the error levels to be expected in the CRRES attitude model. As a general rule of thumb, one can expect accuracy of better than  $2^\circ$  in periods more than two orbits after an attitude adjustment. An attitude adjust orbit may have errors of  $10^\circ$  or so at times after the adjustment. In the following orbits, segments less than about one hour in duration may also exhibit increased error levels as could the eclipse segment if present. Longer segments should for the most part be accurate to  $2^\circ$  or so. Of course, there are exceptions to this due to special events or orbital configurations, including periods of data dropout. In the consideration of accuracy, it is also important to keep in mind that we are discussing the accuracy of an 'average' attitude. Angular deviations due to nutation, in-plane motion, rocking should be added to these estimates. Approximate descriptions of the types of motion to be expected from several maneuvers is given in the next section.

In support of this, we have performed a survey of about 100 orbits, calculating the RMS average and maximum deviation of the measured field from the IGRF model during the first 45 minutes after first perigee. The results are shown in Figure 15.

All of the orbits around 625 and 690 with RMS deviations exceeding  $2^\circ$  are immediately following attitude adjustments. In the 625 series, the adjustments took place approximately two-thirds of the way into the orbit, meaning that the 45 minutes following first perigee of the following orbit was only about one-third orbit after the adjustment. As we have seen, deviation of the spacecraft attitude from pure rotation can account for about  $5^\circ$  or more of this error, so even a perfect model would still fall short by this amount.

In the 690 series, the attitude adjustment took place in the first one-third of the orbit previous to the perigee for which the determination in Figure 15 was made. For these, the lower error level shows the decay of the wire boom motion coupled with increased ability of the model to accurately calculate spin rate changes.

In considering Figure 15, we should also remember that the determination was made, by necessity, near first perigee, which is represented by a short segment. Error levels in the much longer central segment of these orbits would be comparable to those in the perigee segments of orbits for which wire boom motion was not a significant factor, since the fitting of the longer segments averages over the motion of the wire booms.

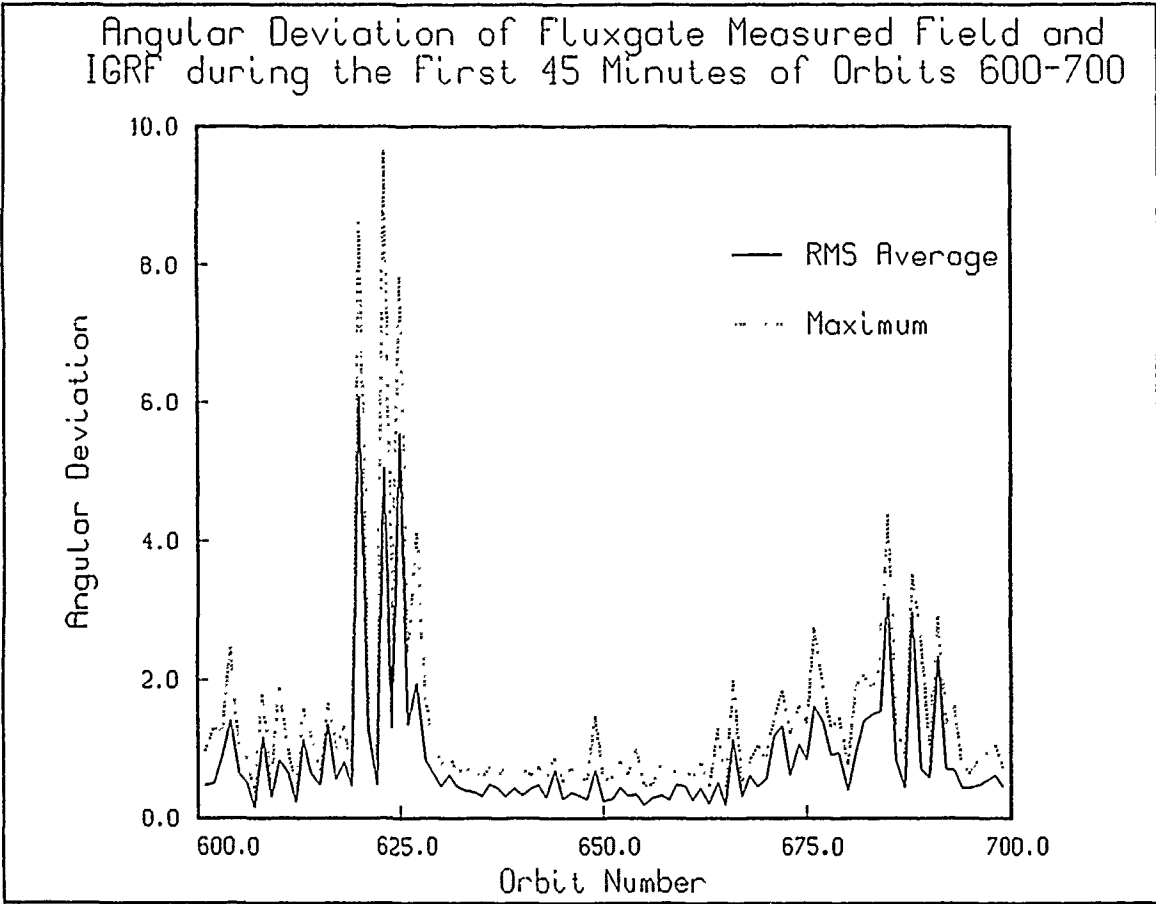


Figure 15. Deviation of the measured from model field during the first 45 minutes of Orbits 600-700.

## 6. ANOMALIES

This section describes several of the non-nominal aspects of the CRRES attitude, arising either from telemetry problems or spacecraft dynamics. The purpose here is to describe generally the motion resulting in the spacecraft. Also included is a more in depth discussion of clock jumps.

### 6.1 CLOCK JUMPS

From time to time, with frequency that depends to some extent on magnetic activity, the spacecraft experiences 'clock jumps' in which the Vehicle Time Correlation Word (VTCW) loses synchronization with the telemetry formatting system. This results in a period of more or less meaningless telemetry until the clock is automatically reset, within a few seconds of the error. This has two important effects on attitude processing. First, since there is often a real time discrepancy between the reset value of the clock and the passage of time, there appears to be a discontinuity in time. For example, sun sensor data timed from the VTCW of each MF might indicate the passage of 40 seconds between sun hits for a single pair of points on either side of the clock jump. All other pairs would be close to the 30 seconds expected at 2 rpm. This is handled in the attitude model by placing a segment near the clock jump. In spite of the fact that the spin phase will be discontinuous at the segment boundary, this method allows the attitude model to match the rest of the science data except for a maximum of 30 seconds before and after the jump. The uncertainty region of maximum 60 seconds arises because the time of the clock jump is determined, as for all mission events effecting attitude, from the attitude data itself. The time resolution of attitude based on a full set of observations is one spin period. Clock jumps are seen as otherwise inexplicable discontinuities in phase. Although more precise times for these jumps are sometimes available from MFF processing, the data at the jump is invariably bad anyway and reliance on attitude data alone streamlines the processing greatly.

A second effect of these jumps is that the absolute UT assigned to a particular MF is less accurate than that of the time correlations from which it is derived. Time correlation factors match a particular VCTW value to actual UT. Thus, if a clock jump happens between two measured correlation factors, the slope of the VCTW to UT conversion becomes incorrect, leading to incorrect UT values. Again, the most sensible way to deal with this appears to be to make the times of the attitude model match the timing of the rest of the data, allowing that the actual time may be up to a few seconds incorrect in some cases. One additional complication arises from the need to relate measured data to ephemeris data, which is timed independently. In only one case so far have we encountered time correlations which were bad enough to cause noticeable discrepancy between measurements and ephemeris models. These few orbits were reprocessed to satisfaction with revised time correlation factors.

## 6.2 ATTITUDE ADJUSTMENTS

Attitude adjustments are carried out frequently to keep the spin axis within  $5^\circ$  and  $15^\circ$  of sun pointing. They lead to strong nutation which can perhaps  $15^\circ$  in magnitude initially. The dominant frequencies are approximately once and twice the spin period. The nutation dampers quench the nutation down to about  $1^\circ$  three hours after the maneuver and to about  $0.1^\circ$  six hours later. Attitude adjusts (and all other maneuvers) are modeled by an 'averaged' attitude in the CRRES software. No attempt is made to model the nutation itself.

The energy transferred to the wire booms by attitude adjustments cause a strong oscillation in the spin axis with a period of approximately 19 minutes. The motion consists mainly of a sort of rocking of the spin axis. The magnitude of the displacement is near the  $10^\circ$  level up to one-half orbit or so following the adjustment. One orbit later it is down to around  $3^\circ$ . It is one-tenth degree three orbits or so later and still visible in magnetic field data six orbits after the adjustment. This motion causes some unique problems in attitude modeling because of its long period. Spin rate changes that occur on timescales of less than one-hour or so are quite difficult to model with high accuracy when the wire boom motion is intense. This is because the spin phase calculated from sun sensor data will show a low frequency oscillation, difficult to separate from the actual spin rate change. Figure 11 shows the magnitude of this interaction quite well.

## 6.3 SPIN RATE CHANGES

Spin rate changes are made whenever the spin rate drifts too far from the nominal 2 rpm, required by several of the science instruments. This maneuver also leads wire boom interaction with a frequency of about 10 Hz. The motion is almost entirely in the spin plane with the spin axis direction unchanged. Since this oscillation is short compared to natural spin rate changes, it does not create particularly severe difficulties for attitude modeling.

## 6.4 CANISTER RELEASES

The effect of the release of canisters from the spacecraft depends on the type and location. Single canister releases generally give rise to nutation which is much like that following attitude adjustments. Dual releases do not in general change the spin axis position. All releases result in spin rate changes, either positive or negative, which have much the same general effects as the spin rate changes induced by the thrusters.

## 6.5 ORBIT ADJUSTS

Orbit adjustments to date have been performed at perigee and have been for the purpose of raising the altitude of apogee. They cause a decrease in the spin rate of substantial magnitude and the same sort of wire boom interactions as do attitude adjustments, though of smaller magnitude.

These anomalies are labeled in the attitude model by codes which are listed in Table 2 below. Of those listed, only the boom deployment has not been used to date. This is because the 20 rpm spin rate of the early portion of the mission was not appropriate for attitude calculation and attitude before orbit 58 was not routinely calculated.

Table 2. Mission Event Codes

0	Normal Segment
1	Spin Up
2	Spin Down
4	Canister Eject
8	Attitude Adjust
16	Boom Deployment
32	Orbit Adjust
64	Begin Eclipse
128	End Eclipse
256	Clock Jump
512	Unspecified Anomaly

## 7. REFERENCES

- Ball Aerospace, "CRRES Attitude Determination and Control Systems Description", Ball SER-3715, Ball Aerospace, Boulder, CO, 1983.
- Ball Aerospace, "Product Function Specification Horizon Sensor - CRRES", Ball Aerospace, Boulder, CO, 1984a.
- Ball Aerospace, "Product Function Specification Sun Sensor - CRRES", Ball Aerospace, Boulder, CO, 1984b.
- Ball Aerospace, "Product Function Specification Magnetometer - CRRES", Ball Aerospace, Boulder, CO, 1984c.
- Ball Aerospace, "Attitude Determination Time-Tagging (Hardware and Software Overview)", SER-3767, Ball Aerospace, Boulder, CO, 1985.
- IMSL, "MATH LIBRARY:FORTTRAN Subroutines for Mathematical Applications", IMSL, Houston, TX, 1987.
- McNeil, W. J., Private communication, April 1990.
- McNeil, W. J. and McInerney, R. E., Private communication, May 1988.
- Wertz, J. R. (ed), "Spacecraft Attitude Determination and Control", JD. Reidel, London, 1986.

## APPENDIX. HISTORY OF MISSION EVENTS

Below is a list of the attitude events that have been encountered through Orbit 800. Numbers in parentheses after the canister releases identify the canister released.

Orbit	Year	Day	Date	UT	Event
058	1990	230	18 Aug	24:04	Attitude Adjust
060	1990	231	19 Aug	19:43	Attitude Adjust
061	1990	232	20 Aug	01:44	Clock Jump
063	1990	232	20 Aug	19:59	Clock Jump
063	1990	233	21 Aug	01:43	Attitude Adjust
066	1990	234	22 Aug	04:51	Attitude Adjust
067	1990	234	22 Aug	16:30	Attitude Adjust
071	1990	236	24 Aug	08:53	Clock Jump
075	1990	237	25 Aug	16:16	Clock Jump
090	1990	244	01 Sep	02:09	Attitude Adjust
091	1990	244	01 Sep	13:27	Attitude Adjust
107	1990	251	08 Sep	03:28	Attitude Adjust
112	1990	253	10 Sep	05:44	Canister Eject (20,44)
122	1990	257	14 Sep	08:19	Canister Eject (18,42)
129	1990	260	17 Sep	03:47	Clock Jump
132	1990	261	18 Sep	04:54	Clock Jump
138	1990	263	20 Sep	21:33	Attitude Adjust
150	1990	268	25 Sep	15:28	Clock Jump
154	1990	270	27 Sep	08:25	Clock Jump
157	1990	271	28 Sep	13:12	Clock Jump
161	1990	273	30 Sep	02:54	Attitude Adjust
164	1990	274	01 Oct	05:09	Attitude Adjust
165	1990	274	01 Oct	22:10	Clock Jump
187	1990	284	11 Oct	01:01	Attitude Adjust
190	1990	285	12 Oct	01:32	Attitude Adjust
199	1990	288	15 Oct	20:29	Clock Jump
199	1990	288	15 Oct	21:21	Clock Jump
209	1990	293	20 Oct	01:00	Clock Jump
210	1990	293	20 Oct	05:59	Attitude Adjust
212	1990	294	21 Oct	06:25	Attitude Adjust
232	1990	302	29 Oct	06:56	Attitude Adjust
234	1990	303	30 Oct	07:57	Attitude Adjust
241	1990	306	02 Nov	03:41	Clock Jump
256	1990	312	08 Nov	01:44	Attitude Adjust
258	1990	312	08 Nov	21:31	Attitude Adjust
274	1990	319	15 Nov	14:12	Clock Jump
278	1990	321	17 Nov	09:28	Attitude Adjust
281	1990	322	18 Nov	07:48	Attitude Adjust
290	1990	325	21 Nov	24:52	Spin Down

291	1990	326	22 Nov	11:17	Spin Down
302	1990	330	26 Nov	23:03	Attitude Adjust
305	1990	332	28 Nov	07:38	Attitude Adjust
310	1990	334	30 Nov	06:38	Clock Jump
317	1990	337	03 Dec	03:10	Attitude Adjust
322	1990	339	05 Dec	06:25	Clock Jump
336	1990	344	10 Dec	23:14	Attitude Adjust
338	1990	345	11 Dec	21:48	Attitude Adjust
342	1990	347	13 Dec	12:35	Unspecified (see 1) <sup>1</sup>
345	1990	348	14 Dec	16:04	Unspecified
360	1990	354	20 Dec	24:07	Attitude Adjust
363	1990	356	22 Dec	04:04	Attitude Adjust
391	1991	002	02 Jan	16:39	Clock Jump
392	1991	003	03 Jan	03:19	Attitude Adjust
395	1991	004	04 Jan	01:43	Attitude Adjust
417	1991	013	13 Jan	01:50	Canister Eject (16)
417	1991	013	13 Jan	06:37	Canister Eject (17,41)
422	1991	015	15 Jan	03:42	Canister Eject (40)
424	1991	016	16 Jan	05:58	Canister Eject (13)
429	1991	018	18 Jan	04:53	Canister Eject (24,48)
434	1991	020	20 Jan	05:03	Canister Eject (21,45)
446	1991	025	25 Jan	01:18	Attitude Adjust
448	1991	026	26 Jan	01:42	Attitude Adjust
451	1991	027	27 Jan	03:05	Attitude Adjust
453	1991	028	28 Jan	02:12	Attitude Adjust
480	1991	039	08 Feb	02:48	Attitude Adjust
482	1991	040	09 Feb	02:53	Attitude Adjust
490	1991	043	12 Feb	03:49	Canister Eject (22,46)
502	1991	048	17 Feb	03:03	Canister Eject (19,43)
524	1991	057	26 Feb	06:28	Attitude Adjust
527	1991	058	27 Feb	06:19	Attitude Adjust
556	1991	070	11 Mar	04:31	Attitude Adjust
558	1991	071	12 Mar	02:37	Attitude Adjust
590	1991	084	25 Mar	02:06	Clock Jump
592	1991	085	26 Mar	04:33	Clock Jump
592	1991	086	27 Mar	04:44	Clock Jump
596	1991	086	27 Mar	14:49	Clock Jump
597	1991	087	28 Mar	04:16	Clock Jump
597	1991	088	29 Mar	05:32	Clock Jump
600	1991	088	29 Mar	04:18	Clock Jump
601	1991	088	29 Mar	13:11	Clock Jump
601	1991	088	29 Mar	14:18	Clock Jump

---

<sup>1</sup> This and the following anomaly have been traced to the failure of one of the batteries. This apparently caused a gas jet leading to a gradual spin rate decrease. The time given is the start of the spin rate change.

788	1991	165	14 Jun	15:39	Spin Up
789	1991	165	14 Jun	18:47	Clock Jump
789	1991	165	14 Jun	21:59	Clock Jump
789	1991	165	14 Jun	22:10	Clock Jump
790	1991	166	15 Jun	05:19	Clock Jump
790	1991	166	15 Jun	13:28	Clock Jump
791	1991	166	15 Jun	15:21	Clock Jump
793	1991	167	16 Jun	11:23	Attitude Adjust
795	1991	168	17 Jun	12:52	Clock Jump
796	1991	168	17 Jun	22:16	Attitude Adjust
796	1991	169	18 Jun	02:12	Clock Jump
797	1991	169	18 Jun	13:11	Clock Jump
799	1991	169	18 Jun	24:59	Clock Jump
799	1991	170	19 Jun	01:16	Attitude Adjust